Odd-frequency pairing inherent in a Bogoliubov Fermi liquid

Tatsuya Miki, Shun-Ta Tamura, Shoma Iimura, and Shintaro Hoshino
Department of Physics, Saitama University, Shimo-Okubo, Saitama 338-8570, Japan

(Received 3 March 2021; revised 31 August 2021; accepted 3 September 2021; published 21 September 2021)

The disorder and interaction effects on Bogoliubov-Fermi surfaces with preserved inversion symmetry are studied for a low-energy effective model coupled to bosonic degrees of freedom. It is shown that the nonideal Bogoliubov quasiparticles (bogolons) generically induce the odd-frequency pair amplitude which reflects a Cooper pairing at different time. The self-energy of bogolons is mainly contributed by the disorder effects in the low frequency limit as in the usual electron liquid. Depending on the choice of the parameters, there are two kinds of solutions: One is frequency independent (but with sign function of frequency) and the other is proportional to the inverse of the frequency, which exist in both the normal and anomalous parts of the self-energy. These characteristic self-energy structures are clearly reflected in the single-particle spectrum. Since the bogolons are originally composed of electrons, the connection between the two is also sought using the concrete $j = 3/2$ fermion model, which reveals that the odd-frequency pairing of bogolons is mainly made of the electrons' odd-frequency pairing.

DOI: 10.1103/PhysRevB.104.094518

I. INTRODUCTION

The superconductivity is induced by the interactions among electrons near the Fermi surfaces. In the resultant ground state, the Cooper pair condensation energy is gained by energy gap formation near the Fermi level. While the Fermi surface usually disappears in the pairing state, they can remain in some superconducting states, where the elementary excitations near the Fermi surfaces are composed of Bogoliubov quasiparticles (bogolons) [1]. The presence of the Fermi surface in superconductors has first been proposed in Ref. [2] and studied in fermionic systems [3–6]. For the time-reversal symmetry broken system with preserved inversion symmetry, such Bogoliubov-Fermi surfaces are stable as they are topologically protected [7,8], which stimulates further theoretical researches in multiorbital systems in recent years [9–13]. Whereas the bogolon is not a simple charged particle, it can carry energy. Hence the thermal properties such as specific heat and thermal conductivity are expected to be similar to the conventional Fermi liquid of electrons [14,15] and are potentially observed in the actual materials [16–18]. However, since the bogolons are quasiparticles in the superconducting state, the physical properties should be different from those of the electrons. Therefore it is desirable to clarify the difference between the Fermi liquid and the *Bogoliubov Fermi liquid*, the latter of which is realized for the nonideal bogolons generically. Recently, the effect of interactions is considered for bogolons and the possible instabilities are studied [19–22]. Here, we show that the impurity and correlation effects on this Bogoliubov Fermi surface generate purely odd-frequency pairing amplitude at low energies, which gives a clear distinction from the normal Fermi liquid state of electrons.

The odd-frequency pairing is proposed as a possible exotic ground state of the fermionic systems where the Cooper pair amplitude has an odd function in relative time or frequency, meaning that the pair formation occurs only at different time [23–32]. The actual realizations as a bulk state have been proposed in correlated electron models [33–35], quasi-one-dimensional system [36,37], geometrically frustrated lattice [38–40], electron-phonon coupled system [41], Kondo lattice [42–46], multichannel Kondo lattice [47–51], and Anderson lattice [52,53]. However, it has been argued that the spatially uniform odd-frequency pairing cannot be a thermodynamically stable state in a conventional framework [54]. Then, several possibilities to remedy this problem are proposed such as spatially modulated superconducting states [43,49,54] and non-Hermitian description with the anomalous relation between the pair amplitude and its conjugate quantity [55–57]. As for the latter scenario, potential problems have also been pointed out [58]. In any case, it has been recognized that the spatially uniform and purely odd-frequency pairing state without conventional (even-frequency) pairing cannot simply be realized. On the other hand, such exotic pairing has been discussed also in edge or interface [59–62], which are secondarily induced from the even-frequency pairing in bulk.

In this paper, we demonstrate the emergence of the spatially uniform odd-frequency pair in the world not of electrons but of bogolons. This odd-frequency pairing is induced by a nonideality of bogolons, where the broken gauge symmetry plays a crucial role as different from the electronic interactions. As shown in the following, the induced odd-frequency pair is closely related to the energy structure of the usual Fermi-liquid self-energy existing in the diagonal Green's function for electrons, but for bogolons it is reflected also in the off-diagonal part, i.e., pair amplitude and pair potential.

In the previous works [19–22], the possibility of the spontaneous symmetry breaking induced by interactions among

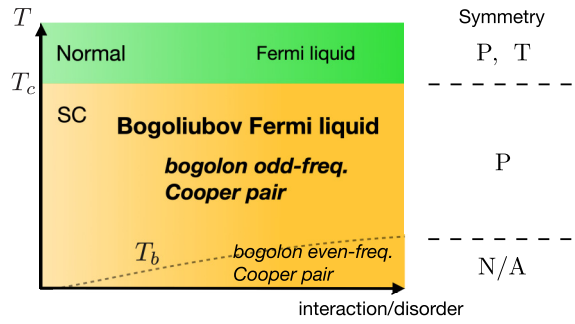

FIG. 1. Schematic phase diagram for the Bogoliubov Fermi liquid. The horizontal axis indicates the deviation from the ideal limit of the bogolons. The dashed line at T_b indicates a possible ordering instability at very low temperature, which may be induced by the attractive interaction among bogolons as discussed in Refs. [19,20]. Note that this paper focuses on $T > T_b$. We assume that the time-reversal symmetry T is broken in the pairing state ($T < T_c$) but the inversion symmetry P is preserved for $T > T_b$.

bogolons is considered. Here, we concentrate on the superconducting state above such low-temperature phase ($T > T_b$) but below the superconducting transition temperature ($T < T_c$). Namely, we deal with a "normal state" of bogolons. Note that the superconducting state has no time-reversal symmetry T, but the inversion symmetry P remains in this temperature regime. Our situation is sketched in Fig. 1.

The remainder of this paper is organized as follows. Section II provides the formulations for the interaction and disorder Hamiltonians of bogolons. The results for disorder are shown in Sec. III. The relation between the original electrons and bogolons is shown in Sec. IV. We summarize the paper in Sec. V. The detailed calculation of the self-energy from the bogolon-boson interaction is given in Appendix A, and the connection between the bogolons and the $j = 3/2$ electrons is summarized in Appendix B.

II. FORMULATION

A. Bogolon and symmetry

Below, we connect the two important concepts of superconductivity, i.e., the Bogoliubov Fermi surface and odd-frequency pairing, based on the concrete model. As in the theories of superconductivity and of Fermi liquid, the degrees of freedom near the Fermi level are important for the low-temperature and low-energy properties. Hence we assume that the dominant contribution enters through the degrees of freedom near the Bogoliubov Fermi surface.

The noninteracting part of the Hamiltonian for bogolons near the Fermi level is written as

$$\mathscr{H}_0 = \sum_{\boldsymbol{k}} \xi_{\boldsymbol{k}} \alpha^\dagger_{\boldsymbol{k}} \alpha_{\boldsymbol{k}}. \tag{1}$$

In the following, we consider the inversion symmetric systems ($\xi_{-\boldsymbol{k}} = \xi_{\boldsymbol{k}}$) with a time-reversal symmetry breaking where the Fermi surface is topologically protected [7]. In order to have an intuition for the energy scales, we write the energy dispersion as $\xi_{\boldsymbol{k}} = \frac{\boldsymbol{k}^2}{2m_b} - \varepsilon_{\mathrm{F}b}$ for simplicity, where m_b and $\varepsilon_{\mathrm{F}b}$ are effective mass and Fermi energy for bogolons ($\hbar = k_{\mathrm{B}} = 1$). As inferred from the original electronic system [7] on which bogolons are based, each quantity is roughly expressed as $m_b \sim \frac{\Delta}{\varepsilon_{\mathrm{F}e}} m_e$ and $\varepsilon_{\mathrm{F}b} \sim \Delta$ where m_e and $\varepsilon_{\mathrm{F}e}$ are mass and Fermi energy for electrons, and Δ is the energy scale for the superconducting gap function. Here we have assumed the magnitude relation $\varepsilon_{\mathrm{F}e} > \Delta$. The Fermi wave number is given by $k_{\mathrm{F}b} = \sqrt{2m_b \varepsilon_{\mathrm{F}b}}$. Thus the Fermi velocity for bogolons is similar to that of electrons: $v_{\mathrm{F}b} = \frac{k_{\mathrm{F}b}}{m_b} \sim v_{\mathrm{F}e}$. Note that the potential term proportional to $\alpha^\dagger_{\boldsymbol{k}} \alpha^\dagger_{-\boldsymbol{k}}$ cannot exist together with the inversion symmetry. Such pair potential may be generated with spontaneous symmetry breaking below the ordering temperature T_b for bogolons as shown in Fig. 1, although we work in the temperature regime $T > T_b$ in the following.

For the superconducting state considered here, the time-reversal and gauge symmetries are assumed to be already broken. Nevertheless, Eq. (1) is invariant for time-reversal-like transformation, i.e., complex conjugation plus $\boldsymbol{k} \to -\boldsymbol{k}$ for spinless bogolon. Also, it has only $\alpha^\dagger \alpha$ like term, which is invariant under the gauge transformation defined by $\alpha_{\boldsymbol{k}} \to \mathrm{e}^{\mathrm{i}\theta} \alpha_{\boldsymbol{k}}$. Hence, in terms of bogolons as in Eq. (1), the effects from these broken symmetries are not described apparently. This paradox at first sight is rationalized by considering the self-energy terms in which the symmetry of the system is reasonably reflected. Then, we arrive at the important conclusion that the anomalous part can be finite in the presence of correlations, and its symmetry must be even-parity pairing. Since the bogolons have no internal degrees of freedom at the Fermi level, and in order to satisfy the Pauli principle, the pairing state of bogolons must have odd relative time dependence. Hence the odd-frequency pairing is reasonably realized. We emphasize that the above argument is based on the symmetry, and the mechanism is generically applicable to the Bogoliubov Fermi surface with inversion symmetry. Hence the target system can be both the bulk and two-dimensional edge, the latter of which is recently proposed in the Weyl semimetal proximately coupled to a superconductor [63].

We further comment on the presence or absence of the internal degrees of freedom of bogolon. Generally in the system with time-reversal symmetry, each band has Kramers degeneracy. If we consider the nodal points in time-reversal-symmetric nodal superconductors, the bogolons have a degenerate band which crosses at the Fermi level and have internal degrees of freedom near the nodal point. Then, the interband pairing is possible, which generically induces the even-frequency pairing. This is in contrast to the cases without internal degrees of freedom studied in this paper.

B. Interaction and disorder Hamiltonians

In order to demonstrate the presence of the odd-frequency pairing in a concrete way, we proceed along with the conventional microscopic approach for the Fermi liquid based on the weak-coupling limit [64]. The total Hamiltonian is written as $\mathscr{H} = \mathscr{H}_0 + \mathscr{H}_{\mathrm{imp}} + \mathscr{H}_{\mathrm{int}}$. The impurity scattering part is given by

$$\mathscr{H}_{\mathrm{imp}} = \frac{1}{V} \sum_{\boldsymbol{k},\boldsymbol{q}} [\rho_{\boldsymbol{q}} u_1(\boldsymbol{k},\boldsymbol{q}) \alpha^\dagger_{\boldsymbol{k}+\boldsymbol{q}} \alpha_{\boldsymbol{k}} + \rho_{\boldsymbol{q}} u_2(\boldsymbol{k},\boldsymbol{q}) \alpha^\dagger_{\boldsymbol{k}+\boldsymbol{q}} \alpha^\dagger_{-\boldsymbol{k}} + \mathrm{H.c.}], \tag{2}$$

where $\rho_{\boldsymbol{q}} = \sum_i e^{i\boldsymbol{q}\cdot\boldsymbol{R}_i}$ is the structure factor for the impurity configuration $\{\boldsymbol{R}_i\}$, and V is a system volume. The second term with $\alpha^\dagger\alpha^\dagger$ is characteristic for the bogolon systems. The quantity $\rho_{\boldsymbol{q}}$ in Eq. (2) satisfies

$$\overline{\rho_{\boldsymbol{q}}\rho_{\boldsymbol{q}'}} = V n_{\rm imp}\delta_{\boldsymbol{q},-\boldsymbol{q}'}, \tag{3}$$

where the overline indicates the average over the impurity configurations and $n_{\rm imp} = V^{-1}\sum_i 1$. The connection to the original electrons is shown in Appendix B 1. We have the relations

$$u_1(\boldsymbol{k},\boldsymbol{q}) = u_1^*(\boldsymbol{k}+\boldsymbol{q},-\boldsymbol{q}), \tag{4}$$

$$u_2(\boldsymbol{k},\boldsymbol{q}) = -u_2(-\boldsymbol{k}-\boldsymbol{q},\boldsymbol{q}), \tag{5}$$

$$u_{1,2}(\boldsymbol{k},\boldsymbol{q}) = u_{1,2}(-\boldsymbol{k},-\boldsymbol{q}), \tag{6}$$

each of which originates from the Hermiticity, Pauli principle (anticommutation relation), and the inversion symmetry after averaging, respectively.

We also consider the correlation effects in $\mathscr{H}_{\rm int}$. Among the various interactions, we take the simple model where the bogolons are coupled with bosons. The interaction term is given by the replacement

$$u_j(\boldsymbol{k},\boldsymbol{q})\rho_{\boldsymbol{q}} \to {\rm i}g_j(\boldsymbol{k},\boldsymbol{q})\sqrt{\frac{\omega_{0,\boldsymbol{q}}}{2}}(b_{\boldsymbol{q}} - b^\dagger_{-\boldsymbol{q}}) \tag{7}$$

in Eq. (2), where $g_{j=1,2}$ is the coupling constant, $\omega_{0,\boldsymbol{q}}$ the bare boson dispersion, and b ($b^\dagger$) the annihilation (creation) operator of boson. Note that, in the above model, we have assumed that the Bogoliubov Fermi surfaces are stable as separated from the other bands located at higher energies. Then, the disorders and interactions dominantly affect the bogolons located near the Bogoliubov Fermi surfaces. Otherwise, the original assumption of the stable Bogoliubov Fermi surfaces must be reconsidered. The above interaction term is derived as a residual interaction originating from the interaction effects on the original electrons. The explicit connection is shown in Appendix B 2. This procedure is similar to the derivation of the effective single-band Hubbard model in cuprate which is originally a multiband system [65].

One may also consider low-energy-lying bosons characteristic for superconductors. While the phase mode is gapped for electronic superconductors due to the long-range nature of the Coulomb interaction, the Higgs mode in anisotropic pairing states can have low excitation energy [66] and may couple to bogolons. In such a case, we can add the contribution from several bosons to the self-energy in the weak-coupling limit, although we expect that the Fermi liquid properties remain qualitatively unchanged.

We note that there also exists the other type of interactions among bogolons without involving bosons [see Eq. (B13) in Appendix B 3]. Although we neglect it for simplicity in this paper, the weak coupling effect might be qualitatively similar to those from bogolon-boson coupling, as expected from the Fermi liquid theory for the electrons [64]. On the other hand, its strong-coupling effects and the possible Fermi-surface instabilities may also be present. The detailed analysis of this interaction is an interesting issue for the future.

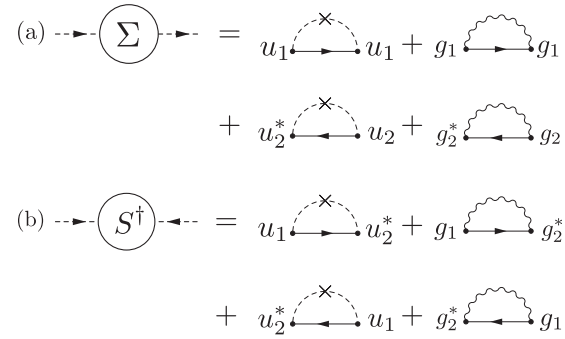

FIG. 2. Diagrams for (a) normal and (b) anomalous self-energies which are relevant to the Bogoliubov Fermi liquid.

C. Self-energies

For concrete analysis, we use the simple weak-coupling perturbation theory, which is a minimal description for the Fermi liquid and is sufficient for generating anomalous Green's functions. The self-energy is contributed by the diagrams shown in Fig. 2, and their calculation is parallel to the usual Fermi liquid theory [64] and is shown in the following and in Appendix A.

The effect of the presence of the odd-frequency pairing is best visualized in the single-particle spectral functions. To see this, we consider the Green's functions given by

$$\begin{aligned}\hat{G}_{\boldsymbol{k}}(\tau) &= \begin{pmatrix} G_{\boldsymbol{k}}(\tau) & F_{\boldsymbol{k}}(\tau) \\ F^\dagger_{\boldsymbol{k}}(\tau) & \bar{G}_{\boldsymbol{k}}(\tau)\end{pmatrix} \\ &= -\left\langle \mathcal{T}\begin{pmatrix}\alpha_{\boldsymbol{k}}(\tau) \\ \alpha^\dagger_{-\boldsymbol{k}}(\tau)\end{pmatrix}(\alpha^\dagger_{\boldsymbol{k}} \quad \alpha_{-\boldsymbol{k}})\right\rangle,\end{aligned} \tag{8}$$

where $\mathcal{T}$ indicates a imaginary time ordering, and $A(\tau) = e^{\tau\mathscr{H}}Ae^{-\tau\mathscr{H}}$ is the Heisenberg picture. Note that the anomalous Green's function becomes nonzero by the $\alpha^\dagger\alpha^\dagger$-like terms in the nonideal Hamiltonians, which are induced by the gauge symmetry breaking [see Eq. (2), Eq. (B8), and Eq. (B13)]. With the phase transformation $\alpha_{\boldsymbol{k}} \to \alpha_{\boldsymbol{k}}e^{i\theta}$, the diagonal Green's function is invariant while the off-diagonal ones change by the factor $e^{2i\theta}$. The anomalous Green's function satisfies $F_{\boldsymbol{k}}(\tau) = -F_{-\boldsymbol{k}}(-\tau)$ and $F_{\boldsymbol{k}}(\tau) = F_{-\boldsymbol{k}}(\tau)$ for the inversion symmetric systems, which leads to the odd-frequency relation $F_{\boldsymbol{k}}(\tau) = -F_{\boldsymbol{k}}(-\tau)$.

The Fourier transformation is defined by

$$\hat{G}_{\boldsymbol{k}}({\rm i}\varepsilon_n) = \int_0^{1/T} d\tau \hat{G}_{\boldsymbol{k}}(\tau)e^{{\rm i}\varepsilon_n\tau}. \tag{9}$$

The normal and anomalous self-energies are introduced by

$$\begin{pmatrix} G_{\boldsymbol{k}} & F_{\boldsymbol{k}} \\ F^\dagger_{\boldsymbol{k}} & \bar{G}_{\boldsymbol{k}}\end{pmatrix}^{-1} = \begin{pmatrix} {\rm i}\varepsilon_n - \xi_{\boldsymbol{k}} & \\ & {\rm i}\varepsilon_n + \xi_{\boldsymbol{k}}\end{pmatrix} - \begin{pmatrix}\Sigma_{\boldsymbol{k}} & S_{\boldsymbol{k}} \\ S^\dagger_{\boldsymbol{k}} & \bar{\Sigma}_{\boldsymbol{k}}\end{pmatrix}, \tag{10}$$

where the frequency dependence is omitted. The self-energies satisfy the relations $\bar{\Sigma}_{\boldsymbol{k}}({\rm i}\varepsilon_n) = -\Sigma^*_{\boldsymbol{k}}({\rm i}\varepsilon_n)$ and $S^\dagger_{\boldsymbol{k}}({\rm i}\varepsilon_n) = -S^*_{\boldsymbol{k}}({\rm i}\varepsilon_n)$ as derived from the Hermiticity and inversion symmetry.

We first consider the lowest-order contribution of the impurity potential. The second-order self-energies (Born approximation) are given as

$$\Sigma_{\boldsymbol{k}}(\mathrm{i}\varepsilon_n) = \Sigma_{1,\boldsymbol{k}}(\mathrm{i}\varepsilon_n) + 2\Sigma_{2,\boldsymbol{k}}(\mathrm{i}\varepsilon_n), \tag{11}$$

$$\Sigma_{1,\boldsymbol{k}}(\mathrm{i}\varepsilon_n) = n_{\mathrm{imp}} \int \frac{d\boldsymbol{q}}{(2\pi)^3} |u_1(\boldsymbol{q}, \boldsymbol{k}-\boldsymbol{q})|^2 G^0_{\boldsymbol{q}}(\mathrm{i}\varepsilon_n), \tag{12}$$

$$\Sigma_{2,\boldsymbol{k}}(\mathrm{i}\varepsilon_n) = -2n_{\mathrm{imp}} \int \frac{d\boldsymbol{q}}{(2\pi)^3} |u_2(\boldsymbol{q}, \boldsymbol{k}-\boldsymbol{q})|^2 G^0_{\boldsymbol{q}}(-\mathrm{i}\varepsilon_n), \tag{13}$$

$$S^\dagger_{\boldsymbol{k}}(\mathrm{i}\varepsilon_n) = -2n_{\mathrm{imp}} \int \frac{d\boldsymbol{q}}{(2\pi)^3} u_1(\boldsymbol{q}, \boldsymbol{k}-\boldsymbol{q}) u_2^*(\boldsymbol{q}, \boldsymbol{k}-\boldsymbol{q}) \times \left[G^0_{\boldsymbol{q}}(-\mathrm{i}\varepsilon_n) - G^0_{\boldsymbol{q}}(\mathrm{i}\varepsilon_n)\right], \tag{14}$$

which corresponds to the diagrams with dotted lines shown in Fig. 2. For the evaluation of the wave-vector integral, we replace the coupling constant by its averaged value with respect to $\boldsymbol{q}$. Then we only have to evaluate the integration as follows:

$$\int \frac{d\boldsymbol{q}}{(2\pi)^3} G^0_{\boldsymbol{q}}(\pm\mathrm{i}\varepsilon_n) = \int \frac{d\boldsymbol{q}}{(2\pi)^3} \frac{1}{\pm\mathrm{i}\varepsilon_n - \xi_{\boldsymbol{q}}} = \mp\mathrm{i}\pi D_0 \mathrm{sgn}\, \varepsilon_n, \tag{15}$$

where D_0 is a density of states of bogolons at the Fermi level. Hence, we obtain the self-energies

$$\Sigma_{\boldsymbol{k}}(\mathrm{i}\varepsilon_n) = -\mathrm{i}\Gamma_{1,\boldsymbol{k}} \mathrm{sgn}\, \varepsilon_n, \tag{16}$$

$$S^\dagger_{\boldsymbol{k}}(\mathrm{i}\varepsilon_n) = -\mathrm{i}\Gamma_{2,\boldsymbol{k}} \mathrm{sgn}\, \varepsilon_n, \tag{17}$$

where

$$\Gamma_{1,\boldsymbol{k}} = \pi n_{\mathrm{imp}} D_0 (\langle |u_1(\boldsymbol{q}, \boldsymbol{k}-\boldsymbol{q})|^2 \rangle_{\boldsymbol{q}} + 4\langle |u_2(\boldsymbol{q}, \boldsymbol{k}-\boldsymbol{q})|^2 \rangle_{\boldsymbol{q}}), \tag{18}$$

$$\Gamma_{2,\boldsymbol{k}} = 4\pi n_{\mathrm{imp}} D_0 \langle u_1(\boldsymbol{q}, \boldsymbol{k}-\boldsymbol{q}) u_2^*(\boldsymbol{q}, \boldsymbol{k}-\boldsymbol{q}) \rangle_{\boldsymbol{q}}, \tag{19}$$

with $\langle \cdots \rangle_{\boldsymbol{q}} = \int d\boldsymbol{q} \cdots / \int d\boldsymbol{q} 1$. One sees that the usual Born approximation result is reproduced if u_2, which is specific to bogolons, is set to zero. We note that $\Gamma_1 > |\Gamma_2|$ is required for the physical behavior, i.e., the positive weight of the spectrum. Indeed, we can show that the condition $|\Gamma_{2,\boldsymbol{k}}| < \Gamma_{1,\boldsymbol{k}}$ is satisfied based on the expressions obtained above together with the magnitude relation between arithmetic and geometric means.

Using the weak-coupling perturbation theory, we also derive the contribution from the interaction with boson in Appendix A. Then the resultant normal part of the self-energy is given by

$$\Sigma_{\boldsymbol{k}}(\mathrm{i}\varepsilon_n) = -\mathrm{i}\Gamma_{1,\boldsymbol{k}} \mathrm{sgn}\, \varepsilon_n + a_{\boldsymbol{k}} \mathrm{i}\varepsilon_n + \mathrm{i}b_{\boldsymbol{k}} \left(\pi^2 T^2 - \varepsilon_n^2\right) \mathrm{sgn}\, \varepsilon_n, \tag{20}$$

where $\varepsilon_n = (2n+1)\pi T$ is the fermionic Matsubara frequency. The explicit coefficients are given in Eqs. (18), (A34), and (A35). The first term corresponds to a quasiparticle damping due to impurity scattering. The second term represents a renormalization factor, and the third term is responsible for the damping in the usual Fermi liquid theory. For bogolons, the anomalous self-energy is also present, whose diagrammatic contribution is very similar to the normal self-energy as shown in Fig. 2(b). The anomalous part is obtained as

$$S^\dagger_{\boldsymbol{k}}(\mathrm{i}\varepsilon_n) = -\mathrm{i}\Gamma_{2,\boldsymbol{k}} \mathrm{sgn}\, \varepsilon_n + c_{\boldsymbol{k}} \mathrm{i}\varepsilon_n + \mathrm{i}d_{\boldsymbol{k}} \left(\pi^2 T^2 - \varepsilon_n^2\right) \mathrm{sgn}\, \varepsilon_n, \tag{21}$$

which is the same frequency dependence as the usual Fermi liquid [see Eqs. (19), (A36), and (A37) for the explicit forms of the coefficients]. Namely, the Fermi-liquid self-energy is originally odd in frequency and therefore it matches well with the requirement of the bogolon anomalous self-energy under the inversion symmetry. This is the reason why the odd-frequency pair potential naturally appears for bogolons. We emphasize that the *spatially uniform and purely odd-frequency pairing* is realized in the present setup, which is necessarily accompanied by the normal self-energies.

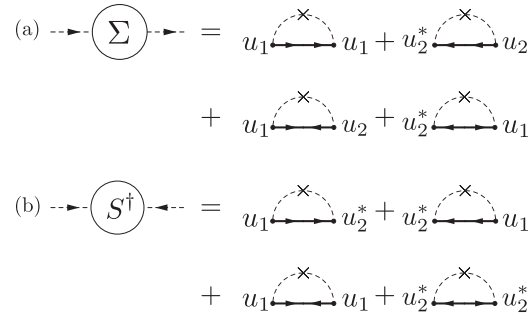

FIG. 3. Feynman diagrams relevant to the self-consistent Born approximation.

From the Hermiticity relation, it can be shown that a, b, and Γ_1 are real, while c, d, and Γ_2 can be complex. As discussed in Ref. [7], the Bogoliubov Fermi surfaces can be realized for a chiral d-wave superconductivity with the gap function $\Delta_{\boldsymbol{k}} \sim k_z(k_x + \mathrm{i}k_y)$ of the original electrons. In this case, the anomalous part c (and also d) may include the contribution $\propto k_z(k_x + \mathrm{i}k_y)$ from the symmetry argument. Hence the broken gauge symmetry and time-reversal symmetry are clearly reflected in the anomalous self-energy of bogolons which is odd in frequency. The symmetries inherent in the nonideal part $\mathscr{H}_0$ in Eq. (1) do not exist in the presence of disorder or interacting part.

III. RESULTS FOR DISORDER

A. Self-consistent treatment

The dominant contribution of the self-energies at low energies enters from the impurity effect. Hence here we focus on the impurity self-energies $\Gamma_{1,2}$ in Eqs. (20) and (21). In the following, we neglect the $\boldsymbol{k}$ dependence in the self-energy for simplicity, corresponding to the spatially local self-energies. For a more accurate analysis of the impurity effect, we consider the self-consistent Born approximation. Namely, we consider the diagrams for the self-energy shown in Fig. 3. The self-consistent equations are derived as

$$\Sigma_{\boldsymbol{k}}(\mathrm{i}\varepsilon_n) = n_{\mathrm{imp}} \int \frac{d\boldsymbol{q}}{(2\pi)^3} [|u_1(\boldsymbol{q}, \boldsymbol{k}-\boldsymbol{q})|^2 G_{\boldsymbol{q}}(\mathrm{i}\varepsilon_n) - 4|u_2(\boldsymbol{q}, \boldsymbol{k}-\boldsymbol{q})|^2 G_{\boldsymbol{q}}(-\mathrm{i}\varepsilon_n) - 2u_1(\boldsymbol{q}, \boldsymbol{k}-\boldsymbol{q}) u_2^*(\boldsymbol{q}, \boldsymbol{k}-\boldsymbol{q}) F_{\boldsymbol{q}}(-\mathrm{i}\varepsilon_n) - 2u_1^*(\boldsymbol{q}, \boldsymbol{k}-\boldsymbol{q}) u_2(\boldsymbol{q}, \boldsymbol{k}-\boldsymbol{q}) F^\dagger_{\boldsymbol{q}}(-\mathrm{i}\varepsilon_n)], \tag{22}$$

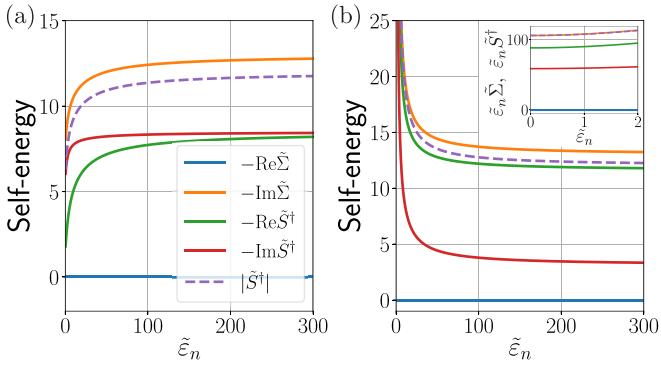

FIG. 4. Examples of the solutions of Eqs. (24) and (25). We define dimensionless self-energies and frequency as $\tilde{\Sigma} = \Sigma/(\pi n_{\mathrm{imp}} D_0 |u_2|^2)$, $\tilde{S}^{\dagger} = S^{\dagger}/(\pi n_{\mathrm{imp}} D_0 |u_2|^2)$, $\tilde{\varepsilon}_n = \varepsilon_n/(\pi n_{\mathrm{imp}} D_0 |u_2|^2)$. The parameters are chosen as (a) $u_1/|u_2| = 3\exp(\mathrm{i}\pi/6)$, $\arg u_2 = \pi/12$ and (b) $u_1/|u_2| = 3\exp(\mathrm{i}\pi/3)$, $\arg u_2 = \pi/12$. The inset shows the self-energy with ε_n multiplied, indicating $-\varepsilon_n \mathrm{Im}\,\Sigma(\mathrm{i}\varepsilon_n) = \varepsilon_n |S^{\dagger}(\mathrm{i}\varepsilon_n)|$ for $\varepsilon_n \to 0$.

$$
\begin{aligned}
S_{\boldsymbol{k}}^{\dagger}(\mathrm{i}\varepsilon_n) = n_{\mathrm{imp}} \int \frac{d\boldsymbol{q}}{(2\pi)^3} [&2u_1^*(\boldsymbol{q}, \boldsymbol{k}-\boldsymbol{q}) u_2^*(\boldsymbol{q}, \boldsymbol{k}-\boldsymbol{q}) \\
&\times (G_{\boldsymbol{q}}(\mathrm{i}\varepsilon_n) - G_{\boldsymbol{q}}(-\mathrm{i}\varepsilon_n)) \\
&+ \tfrac{1}{2} u_1^*(\boldsymbol{q}, \boldsymbol{k}-\boldsymbol{q}) u_1^*(\boldsymbol{q}, \boldsymbol{k}-\boldsymbol{q}) (F_{\boldsymbol{q}}^{\dagger}(\mathrm{i}\varepsilon_n) - F_{\boldsymbol{q}}^{\dagger}(-\mathrm{i}\varepsilon_n)) \\
&+ 2u_2^*(\boldsymbol{q}, \boldsymbol{k}-\boldsymbol{q}) u_2^*(\boldsymbol{q}, \boldsymbol{k}-\boldsymbol{q}) (F_{\boldsymbol{q}}(\mathrm{i}\varepsilon_n) - F_{\boldsymbol{q}}(-\mathrm{i}\varepsilon_n))].
\end{aligned} \tag{23}
$$

Obviously, these equations reduce to those in the Born approximation in the last subsection if one drops the self-energies in the right-hand side. In order to search for the concrete solutions, we simplify the equation by replacing the coefficients by the wave-vector independent ones, and then the self-energies are also $\boldsymbol{k}$ independent. We have considered all the parameter space within this approximation and always have found physical solutions. Defining the energy-dependent functions $\Gamma_{1,2}(\mathrm{i}\varepsilon_n)$ by $\Sigma(\mathrm{i}\varepsilon_n) = -\mathrm{i}\Gamma_1(\mathrm{i}\varepsilon_n)$ and $S^{\dagger}(\mathrm{i}\varepsilon_n) = -\mathrm{i}\Gamma_2(\mathrm{i}\varepsilon_n)$, we obtain the equations

$$
\begin{aligned}
\Gamma_1(\mathrm{i}\varepsilon_n) = &\frac{\mathrm{i}\pi n_{\mathrm{imp}} D_0}{\sqrt{-(\varepsilon_n + \mathrm{Re}\Gamma_1(\mathrm{i}\varepsilon_n))^2 + |\Gamma_2(\mathrm{i}\varepsilon_n)|^2}} \\
&\times [(|u_1|^2 + 4|u_2|^2)(\varepsilon_n + \mathrm{Re}\Gamma_1(\mathrm{i}\varepsilon_n)) \\
&- 2u_1 u_2^* \Gamma_2^*(i\varepsilon_n) - 2u_1^* u_2 \Gamma_2(\mathrm{i}\varepsilon_n)]
\end{aligned} \tag{24}
$$

$$
\begin{aligned}
\Gamma_2(\mathrm{i}\varepsilon_n) = &\frac{\mathrm{i}\pi n_{\mathrm{imp}} D_0}{\sqrt{-(\varepsilon_n + \mathrm{Re}\Gamma_1(\mathrm{i}\varepsilon_n))^2 + |\Gamma_2(\mathrm{i}\varepsilon_n)|^2}} \\
&\times [4u_1^* u_2^* (\varepsilon_n + \mathrm{Re}\Gamma_1(\mathrm{i}\varepsilon_n)) \\
&- u_1^* u_1^* \Gamma_2(i\varepsilon_n) - 4u_2^* u_2^* \Gamma_2^*(\mathrm{i}\varepsilon_n)].
\end{aligned} \tag{25}
$$

Performing a suitable transformation for the dimensionless expressions of the equations, we find that the equations are controlled by the complex parameter $u_1/|u_2|$. We note that the solution is identical to the Born approximation discussed in the last subsection at high frequencies.

We can solve the above simultaneous equations at each frequency. The calculation examples are shown in Fig. 4, where we have the two kinds of solutions depending on the parameters both of which are odd function in frequency or imaginary time.

(i) Solution of the first kind: The characteristic behaviors are seen in the low-energy limit $\varepsilon_n \to 0$. The first kind has the form

$$
\Sigma(\mathrm{i}\varepsilon_n \to 0) = -\mathrm{i}\Gamma_1 \mathrm{sgn}\,\varepsilon_n, \tag{26}
$$

$$
S^{\dagger}(\mathrm{i}\varepsilon_n \to 0) = -\mathrm{i}\Gamma_2 \mathrm{sgn}\,\varepsilon_n, \tag{27}
$$

which is similar to the results in the simple Born approximation. We can explicitly obtain the solution as

$$
\frac{\Gamma_2}{\Gamma_1} = \begin{cases} \frac{2u_2^*}{\mathrm{Re}u_1} & (2 < |\mathrm{Re}u_1|/|u_2|), \\ \frac{\mathrm{Re}u_1}{2u_2} & (\mathrm{Im}u_1/|u_2| = 0 \text{ and } 0 < |\mathrm{Re}u_1|/|u_2| < 2) \end{cases} \tag{28}
$$

for $|\mathrm{Re}\,u_1|/|u_2| > 2$ or $\mathrm{Im}\,u_1/|u_2| = 0$. The calculation example is shown in Fig. 4(a).

(ii) Solution of the second kind: On the other hand, owing to the nonlinearity of the equations, we have also found another type of solution depending on the choice of the parameters. This solution of the second kind is obtained for $|\mathrm{Re}\,u_1|/|u_2| < 2$ and $\mathrm{Im}\,u_1/|u_2| \neq 0$, which has the frequency dependence

$$
\Sigma(\mathrm{i}\varepsilon_n \to 0) = \frac{|V|^2}{\mathrm{i}\varepsilon_n}, \tag{29}
$$

$$
S^{\dagger}(\mathrm{i}\varepsilon_n \to 0) = \frac{V^2}{\mathrm{i}\varepsilon_n}, \tag{30}
$$

where V is a complex constant. The calculation example is shown in Fig. 4(b). In this case, we have the three single-particle excitation energies $E_{\boldsymbol{k}} = 0, \pm\sqrt{\xi_{\boldsymbol{k}}^2 + 2|V|^2}$ from the pole of Green's functions. This energy structure is due to the fact that the same absolute value of $|V|$ is shared for both the normal and anomalous part of self-energy. The absolute value $|V|$ cannot be written in the simple analytic form but is determined easily from the numerical calculations.

The frequency dependence proportional to the inverse of ε_n for both the normal and anomalous parts are the same features as the pairing states in the multichannel Kondo lattices where the conduction electrons hybridized virtually with the localized fermions [43,50,67–69]. This suggests that the $1/\varepsilon_n$ form is a ubiquitous form of the self-energy for odd-frequency pairing in bulk, as it is found in the very different two possible physical systems.

B. Single-particle spectral functions

From the normal and anomalous Green's functions, we obtain several physical quantities of interest. The first one is the single-particle spectral function and density of states defined by

$$
A_{\boldsymbol{k}}(\varepsilon) = -\frac{1}{\pi} \mathrm{Im}\, G_{\boldsymbol{k}11}(\varepsilon + \mathrm{i}\eta), \tag{31}
$$

$$
D(\varepsilon) = \sum_{\boldsymbol{k}} A_{\boldsymbol{k}}(\varepsilon) \simeq D_0 \int d\xi_{\boldsymbol{k}} A_{\boldsymbol{k}}(\varepsilon). \tag{32}
$$

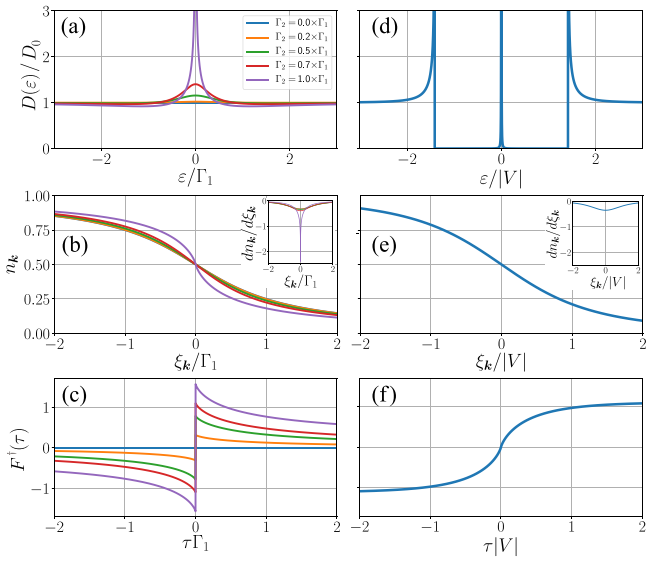

FIG. 5. (a) Density of states, (b) momentum distribution function, (c) pair potential for the solution of the first kind. (d), (e), and (f) are similar to (a), (b), and (c), respectively, but for the solution of the second kind. D_0 is a bare density of states. The pair amplitude in (c) is normalized by $\Gamma_1 D_0$ and in (f) by $|V|D_0$ where the phases are chosen as zero.

The momentum distribution function is given by

$$n_{\boldsymbol{k}} = \langle \alpha_{\boldsymbol{k}}^\dagger \alpha_{\boldsymbol{k}} \rangle. \tag{33}$$

In addition, the time-dependent pair amplitude can also be calculated. Whereas the static quantity such as $\langle \alpha_{\boldsymbol{k}} \alpha_{-\boldsymbol{k}} \rangle$ is zero due to the inversion symmetry, the pair amplitude is finite at different times. Specifically we consider the spatially local quantity

$$F(\tau) = T \sum_{n,\boldsymbol{k}} F_{\boldsymbol{k}}(\mathrm{i}\varepsilon_n) \mathrm{e}^{-\mathrm{i}\varepsilon_n \tau}. \tag{34}$$

These quantities will be graphically shown later in Fig. 5.

Another interesting quantity is the radius of the odd-frequency Cooper pair. We consider the pair amplitude with spatiotemporal dependence:

$$F(\boldsymbol{r}, \tau) = T \sum_{n,\boldsymbol{k}} F_{\boldsymbol{k}}(\mathrm{i}\varepsilon_n) \mathrm{e}^{\mathrm{i}\boldsymbol{k}\cdot\boldsymbol{r} - \mathrm{i}\varepsilon_n \tau}. \tag{35}$$

Evaluating this quantity at $r \to \infty$ limit. We can define the pair radius l by $F(\boldsymbol{r}, \tau) \sim \mathrm{e}^{-r/l}$.

The information of quasiparticles are also seen in the real-time evolution of the retarded Green's function, which is given by

$$G^{\mathrm{R}}(t) = -\mathrm{i}\theta(t) \langle \{ \alpha_{\boldsymbol{k}}(t), \alpha_{\boldsymbol{k}}^\dagger \} \rangle, \tag{36}$$

where $\theta(t)$ is the step function. Here we have considered the real-time Heisenberg picture $A(t) = \mathrm{e}^{\mathrm{i}t\mathscr{H}} A \mathrm{e}^{-\mathrm{i}t\mathscr{H}}$. In the following, we summarize the above physical quantities for the solutions of both the first and second kinds.

(i) Solution of the first kind: We consider the self-energies at low energy limit given in Eqs. (26) and (27):

$$\Sigma(\mathrm{i}\varepsilon_n) = -\mathrm{i}\Gamma_1 \mathrm{sgn}\, \varepsilon_n, \quad S^\dagger(\mathrm{i}\varepsilon_n) = -\mathrm{i}\Gamma_2 \mathrm{sgn}\, \varepsilon_n, \tag{37}$$

with $\Gamma_1 > |\Gamma_2|$. The density of states is

$$\frac{D(\varepsilon)}{D_0} = \frac{|\varepsilon| + \mathrm{i}\Gamma_1}{2\sqrt{(|\varepsilon| + \mathrm{i}\Gamma_1)^2 + |\Gamma_2|^2}} + \mathrm{c.c.}, \tag{38}$$

which is shown in Fig. 5(a). The larger Γ_2 makes the higher peak at the Fermi level. Clearly, the presence of odd-frequency pair is responsible for this characteristic feature near the Fermi level.

The momentum distribution function is

$$n_{\boldsymbol{k}} = \frac{\xi_{\boldsymbol{k}}}{2\pi\sqrt{|\Gamma_2|^2 - \xi_{\boldsymbol{k}}^2}} \ln \left(\frac{\Gamma_1 - \sqrt{|\Gamma_2|^2 - \xi_{\boldsymbol{k}}^2}}{\Gamma_1 + \sqrt{|\Gamma_2|^2 - \xi_{\boldsymbol{k}}^2}} \right) + \frac{1}{2} \tag{39}$$

at zero temperature, which is shown in Fig. 5(b). The sharp drop at the Fermi energy in the ideal limit is smeared by the damping Γ_1 but is gradually recovered with increasing $|\Gamma_2|$. The inset of (b) shows the derivative of this function, where the change becomes more abrupt for the larger pair potential Γ_2 and diverges when $|\Gamma_2| \to \Gamma_1$.

The spatially local pair amplitude at $T = 0$ is

$$\frac{F^\dagger(\tau)}{\Gamma_2 D_0} = \int_0^\infty d\varepsilon \left[\frac{\mathrm{i}}{2\sqrt{(|\varepsilon| + \mathrm{i}\Gamma_1)^2 + |\Gamma_2|^2}} + \mathrm{c.c.} \right] \mathrm{e}^{-\varepsilon\tau} \tag{40}$$

for $\tau > 0$, which is numerically integrated. We show the τ dependence of Eq. (40) in Fig. 5(c). The functional form with respect to time clearly shows the odd-frequency pairing. The value of the pair amplitude is largest at short time and is discontinuous at $\tau = 0$. The asymptotic behavior at long time is $F^\dagger(\tau \to \infty) \sim \tau^{-1}$.

Next, we consider the radius of Cooper pair. The pair amplitude for $r \to \infty$ limit is explicitly evaluated in a manner similar to the standard BCS theory [70]. Assuming that the contributions from the Fermi surface are dominant, we perform the wave-vector integral and obtain

$$F^\dagger(\boldsymbol{r}, \tau) = \pi T D_0 \mathrm{i}\Gamma_2 \sum_n \frac{\mathrm{sgn}\, \varepsilon_n}{\sqrt{(|\varepsilon_n| + \Gamma_1)^2 - |\Gamma_2|^2}} \frac{k_{\mathrm{F}b} \sin(k_{\mathrm{F}b} r) - \left(\sqrt{(|\varepsilon_n| + \Gamma_1)^2 - |\Gamma_2|^2/\Gamma_1^2}/v_{\mathrm{F}b} \right) \cos(k_{\mathrm{F}b} r)}{\left[k_{\mathrm{F}b}^2 + [(|\varepsilon_n| + \Gamma_1)^2 - |\Gamma_2|^2]/v_{\mathrm{F}b}^2 \right] r}$$

$$\times\, \mathrm{e}^{-i\varepsilon_n \tau} \exp(-\sqrt{(|\varepsilon_n| + \Gamma_1)^2 - |\Gamma_2|^2} r/v_{\mathrm{F}b}). \tag{41}$$

Taking the zero-temperature limit, the asymptotic form is given by

$$F^{\dagger}(\boldsymbol{r},\tau)\sim 2\pi T\Gamma_2 D_0\sin(\pi T\tau)\frac{k_{Fb}\sin(k_{Fb}r)-\left(\sqrt{\Gamma_1^2-|\Gamma_2|^2}/v_{Fb}\right)\cos(k_{Fb}r)}{\sqrt{\Gamma_1^2-|\Gamma_2|^2}\left(k_{Fb}^2+\left[\Gamma_1^2-|\Gamma_2|^2\right]/v_{Fb}^2\right)r}\exp\left(-\sqrt{\Gamma_1^2-|\Gamma_2|^2}r/v_{Fb}\right). \tag{42}$$

Therefore, we obtain the pair radius at zero temperature limit

$$l=\frac{v_{Fb}}{\sqrt{\Gamma_1^2-|\Gamma_2|^2}}. \tag{43}$$

Namely, whereas the single-particle gap is absent in the systems with Bogoliubov Fermi surfaces, the characteristic length, i.e., the pair radius, is finite. The length extends with increasing the odd-frequency pair potential Γ_2.

We also take a look at the real time dependence of the retarded Green's function ($t>0$), which is given by

$$G_{\boldsymbol{k}}^{R}(t)=-\frac{i}{2}\left(1+\frac{\xi_{\boldsymbol{k}}}{\sqrt{\xi_{\boldsymbol{k}}^2-|\Gamma_2|^2}}\right)e^{-i\sqrt{\xi_{\boldsymbol{k}}^2-|\Gamma_2|^2}t-\Gamma_1 t}-\frac{i}{2}\left(1-\frac{\xi_{\boldsymbol{k}}}{\sqrt{\xi_{\boldsymbol{k}}^2-|\Gamma_2|^2}}\right)e^{i\sqrt{\xi_{\boldsymbol{k}}^2-|\Gamma_2|^2}t-\Gamma_1 t} \tag{44}$$

for $|\xi_{\boldsymbol{k}}|>|\Gamma_2|$ and

$$G_{\boldsymbol{k}}^{R}(t)=-\frac{1}{2}\left(i+\frac{\xi_{\boldsymbol{k}}}{\sqrt{|\Gamma_2|^2-\xi_{\boldsymbol{k}}^2}}\right)e^{-(\Gamma_1-\sqrt{|\Gamma_2|^2-\xi_{\boldsymbol{k}}^2})t}-\frac{1}{2}\left(i-\frac{\xi_{\boldsymbol{k}}}{\sqrt{|\Gamma_2|^2-\xi_{\boldsymbol{k}}^2}}\right)e^{-(\Gamma_1+\sqrt{|\Gamma_2|^2-\xi_{\boldsymbol{k}}^2})t} \tag{45}$$

for $|\xi_{\boldsymbol{k}}|<|\Gamma_2|$. Therefore, for the high-energy region with $\xi_{\boldsymbol{k}}>|\Gamma_2|$, the complex energy $z_{\boldsymbol{k}}$, which is defined by $G_{\boldsymbol{k}}^{R}(t)\sim e^{iz_{\boldsymbol{k}}t}$, is given by $z_{\boldsymbol{k}}=\pm\sqrt{\xi_{\boldsymbol{k}}^2-|\Gamma_2|^2}+i\Gamma_1$. This is a standard form composed of the oscillating part with the quasiparticle energy $\sqrt{\xi_{\boldsymbol{k}}^2-|\Gamma_2|^2}$ and the damping Γ_1. On the contrary, for $\xi_{\boldsymbol{k}}<|\Gamma_2|$, we have $z_{\boldsymbol{k}}=i(\pm\sqrt{|\Gamma_2|^2-\xi_{\boldsymbol{k}}^2}+\Gamma_1)$ which is purely imaginary. Hence the low-energy part has no oscillating part and has only damping with two relaxation rates.

(ii) Solution of the second kind: Here, we summarize the results for the self-energies given in Eqs. (29) and (30):

$$\Sigma(i\varepsilon_n)=|V|^2/i\varepsilon_n,\quad S^{\dagger}(i\varepsilon_n)=V^2/i\varepsilon_n. \tag{46}$$

The density of states is

$$\frac{D(\varepsilon)}{D_0}=\frac{\pi}{\sqrt{2}}|V|\delta(\varepsilon)+\frac{\varepsilon^2-|V|^2}{\varepsilon\sqrt{\varepsilon^2-2|V|^2}}\theta(\varepsilon-\sqrt{2}|V|). \tag{47}$$

The presence of the gap structure and the zero-energy peak at the Fermi level is the characteristic feature for the density of states as shown in Fig. 5(d), where the weight of the zero-energy peak is proportional to $|V|$. The sharp peak inside the gap in the density of states is reminiscent of the impurity bound state. However, it is difficult within the weak-coupling perturbation theory to conclude that this in-gap state is the impurity bound state, since the bound state is connected with the real-space picture in the strong coupling limit.

The momentum distribution function is

$$n_{\boldsymbol{k}}=\frac{E_{\boldsymbol{k}}-\xi_{\boldsymbol{k}}[1-2f(E_{\boldsymbol{k}})]}{2E_{\boldsymbol{k}}}, \tag{48}$$

where $E_{\boldsymbol{k}}=\sqrt{\xi_{\boldsymbol{k}}^2+2|V|^2}$ and $f(x)=1/(e^{x/T}+1)$. The spatially local pair amplitude is

$$\frac{F^{\dagger}(\tau)}{VD_0}=\frac{\pi V}{2\sqrt{2}|V|}-V\int_{\sqrt{2}|V|}^{\infty}d\varepsilon\frac{e^{-\varepsilon\tau}}{\varepsilon\sqrt{\varepsilon^2-2|V|^2}} \tag{49}$$

for $\tau>0$, which is numerically integrated. Figures 5(e) and 5(f) show the momentum distribution function and imaginary-time dependence of local pair amplitude, respectively, for the case with the second kind. The pair amplitude has odd function form but is now smooth at equal imaginary time. The asymptotic behaviors are identified as $F^{\dagger}(\tau)\sim -|V|^2\tau\ln(\tau|V|)$ for $\tau\to 0$ and $F^{\dagger}(\tau)\sim|V|$ for $\tau\to\infty$.

The Cooper pair radius is evaluated from the pair amplitude for $r\to\infty$ limit:

$$F^{\dagger}(\boldsymbol{r},\tau)\sim 2D_0V^2\sin(\pi T\tau)\times\frac{[k_{Fb}\sin(k_{Fb}r)-(\sqrt{2}|V|/v_{Fb})\cos(k_{Fb}r)]}{\sqrt{2}|V|\left(k_{Fb}^2+2|V|^2/v_{Fb}^2\right)r}e^{-\sqrt{2}|V|r/v_{Fb}}, \tag{50}$$

where we have taken $T\to 0$ limit. Then we obtain the pair radius at zero temperature limit as

$$l=\frac{v_{Fb}}{\sqrt{2}|V|}. \tag{51}$$

The real time dependence of the Green's function is given by

$$G_{\boldsymbol{k}}^{R}(t)=-\frac{i}{2E_{\boldsymbol{k}}^2}\left[2|V|^2+\left(\xi_{\boldsymbol{k}}^2+|V|^2+\xi_{\boldsymbol{k}}E_{\boldsymbol{k}}\right)e^{-iE_{\boldsymbol{k}}t}+\left(\xi_{\boldsymbol{k}}^2+|V|^2-\xi_{\boldsymbol{k}}E_{\boldsymbol{k}}\right)e^{iE_{\boldsymbol{k}}t}\right] \tag{52}$$

for $t>0$.

C. Relevance to real materials

Let us make a comment on the relevance to real materials. The Bogoliubov Fermi liquid shows characteristic single-particle excitations at low energies, which can be much different from the usual electron liquids. As discussed in the last subsections, the above two different behaviors, the first- and second-kind solutions, are observed depending on the choice of parameters and hence are dependent on the specific materials. For example, in Fe(Se,S), the Fermi-liquid-like behavior is observed below the superconducting transition temperature as probed by thermal measurement [16,18]. The

solution of the second kind shows the presence of the localized level at the Fermi level, which should not contribute to the transport phenomena. Hence, the solution of the first kind with the form (21) is likely realized in Fe(Se,S). While the observed behaviors are similar to the Fermi liquid and the quantum oscillation is observed [71], which implies weak disorder effects, the tuning of the system may make it clearer to detect the fingerprints of Bogoliubov-Fermi liquids. In this way, a careful study on the single-particle spectral functions can capture the physics of the odd-frequency pairing.

IV. RELATION BETWEEN ELECTRONIC HAMILTONIAN AND BOGOLONS

We discuss the connection of the bogolon degrees of freedom to original electrons. As a simple realization of the Bogoliubov Fermi surface, we take the $j = 3/2$ fermion model proposed in Ref. [7], where the symmetric spin-orbit interaction and time-reversal-symmetry-broken $d + id$ pairing are considered. The Hamiltonian is given by [7,20]

$$\mathscr{H} = \sum_{\boldsymbol{k}} \vec{c}_{\boldsymbol{k}}^{\dagger}\left[\left(\frac{\boldsymbol{k}^2}{2m_e} - \varepsilon_{\mathrm{Fe}}\right)\hat{1} + \beta(\boldsymbol{k}\cdot\hat{\boldsymbol{J}})^2\right]\vec{c}_{\boldsymbol{k}} + \sum_{\boldsymbol{k}} \vec{c}_{\boldsymbol{k}}^{\dagger}\left[\Delta_1 k_z(k_x + \mathrm{i}k_y)\hat{E} + \frac{2\Delta_0}{\sqrt{3}}\lceil\hat{J}_z(\hat{J}_x + \mathrm{i}\hat{J}_y)\rfloor\hat{E}\right]\vec{c}_{-\boldsymbol{k}}^{\dagger\mathrm{T}} + \mathrm{H.c.}, \tag{53}$$

where $\vec{c}_{\boldsymbol{k}} = (c_{\boldsymbol{k},3/2}, c_{\boldsymbol{k},1/2}, c_{\boldsymbol{k},-1/2}, c_{\boldsymbol{k},-3/2})^{\mathrm{T}}$ is the spin 3/2 spinor of electrons. The vector $\hat{\boldsymbol{J}}$, which is 4×4 matrix, represents a spin-3/2 operator (or dipole), and $\hat{E}$ is the antisymmetric matrix defined in Ref. [20]. The square bracket symmetrizes the product of matrices as $\lceil\hat{A}\hat{B}\rfloor = (\hat{A}\hat{B} + \hat{B}\hat{A})/2$.

The time-reversal-symmetry broken superconducting state with inversion symmetry generally realizes the Bogoliubov-Fermi surfaces which are topologically protected [7]. Then the resultant effective low-energy Hamiltonian in Eq. (1) is derived and the bogolon operators are given by

$$\alpha_{\boldsymbol{k}} = \sum_m (u_{\boldsymbol{k},m}c_{\boldsymbol{k},m} + v_{\boldsymbol{k},m}c_{-\boldsymbol{k},m}^{\dagger}), \tag{54}$$

where the coefficients u and v are obtained by diagonalizing the Hamiltonian Eq. (53). The odd-frequency pair amplitude of bogolons is now defined by

$$F_{\boldsymbol{k}}(\tau) = -\langle\mathcal{T}\alpha_{\boldsymbol{k}}(\tau)\alpha_{-\boldsymbol{k}}\rangle, \tag{55}$$

which is an odd function with respect to time and is induced from the disorder and correlation effects.

The pair amplitude of bogolons is connected to the order parameters of the original electrons. At each $\boldsymbol{k}$ point on the Fermi surface, we can define the electronic multipoles $M_{\boldsymbol{k}}^r$ and multiplet pair amplitudes $P_{\boldsymbol{k}}^r$, $P_{\boldsymbol{k}}^{\dagger,r}$, which are classified by the rank r defined up to $2j$. We define the time-dependent order parameters in terms of the original electrons as

$$M_{\boldsymbol{k}}^{\eta}(\tau) = \langle\mathcal{T}\vec{c}_{\boldsymbol{k}}^{\dagger}\hat{O}^{\eta}\vec{c}_{\boldsymbol{k}}(\tau)\rangle, \tag{56}$$

$$P_{\boldsymbol{k}}^{\eta}(\tau) = \left\langle\mathcal{T}\vec{c}_{\boldsymbol{k}}^{\dagger}\hat{O}^{\eta}\hat{E}\vec{c}_{-\boldsymbol{k}}^{\dagger\mathrm{T}}(\tau)\right\rangle, \tag{57}$$

TABLE I. List of the types of diagonal and off-diagonal physical quantities classified by the rank r. See Ref. [20] for the detailed forms of the matrices $\hat{O}^{\eta}$.

Rank	η
$r = 0$ (monopole/singlet)	1
$r = 1$ (dipole/triplet)	x, y, z
$r = 2$ (quadrupole/quintet)	$xy, yz, zx, z^2, x^2 - y^2$
$r = 3$ (octupole/septet)	$xyz, xz^2, yz^2, z^3, z(x^2 - y^2)$, $x(x^2 - 3y^2), y(3x^2 - y^2)$

$$P_{\boldsymbol{k}}^{\dagger\eta}(\tau) = \left\langle\mathcal{T}\vec{c}_{-\boldsymbol{k}}^{\mathrm{T}}(\hat{O}^{\eta}\hat{E})^{\dagger}\vec{c}_{\boldsymbol{k}}(\tau)\right\rangle. \tag{58}$$

The 4×4 matrices $\hat{O}^{\eta}$ are defined in Ref. [20], where all the order parameters are exhausted by this expression. The pair amplitude corresponds to the multiplet pairs, i.e., electron (P) and hole ($P^{\dagger}$) pair amplitudes. The index η represents an identifier for the multipoles and multiplet pairs (note that the symbol η in this paper corresponds to η' in Ref. [20]). For the diagonal quantity, $r = 0, 1, 2, 3$ corresponds to one monopole, three dipoles, five quadrupole, and seven octupole. For the off-diagonal quantity, $r = 0, 1, 2, 3$ correspond to singlet, triplet, quintet, and septet pairs. We list possible indices in Table I.

The time-dependent multipole functions are represented in terms of bogolon's physical quantities. In order to see the contributions from the odd-frequency pairing of bogolons near the Fermi level, we define the odd-frequency multipoles $\tilde{M}^{\eta}$, $\tilde{P}^{\eta}$, $\tilde{P}^{\dagger\eta}$ which are induced solely by the degrees of freedom near the Bogoliubov Fermi surfaces and are written in the forms

$$\tilde{M}_{\boldsymbol{k}}^{\eta}(\tau) = C_M^{\eta}(\boldsymbol{k})F_{\boldsymbol{k}}(\tau), \tag{59}$$

$$\tilde{P}_{\boldsymbol{k}}^{\eta}(\tau) = C_P^{\eta}(\boldsymbol{k})F_{\boldsymbol{k}}(\tau), \tag{60}$$

$$\tilde{P}_{\boldsymbol{k}}^{\dagger\eta}(\tau) = C_{P^{\dagger}}^{\eta}(\boldsymbol{k})F_{\boldsymbol{k}}(\tau). \tag{61}$$

The quantity C is regarded as a kind of 'susceptibility,' showing how much of odd-frequency multipoles and multiplet pair of electrons are induced from the odd-frequency pair amplitude of bogolons. We then define the quantities depending only on the rank

$$C_X^r(\boldsymbol{k}) = \sqrt{\sum_{\eta\in r}\left|C_X^{\eta}(\boldsymbol{k})\right|^2} \tag{62}$$

for $X = M, P, P^{\dagger}$. For the multiplet pairs, only the spin-triplet and spin-septet pair can be finite due to the odd function in time in systems with inversion symmetry.

Figure 6 shows the value of C_X along the Fermi surface. For exemplary demonstration, we take the parameters as the symmetric spin-orbit coupling $\beta/\varepsilon_{\mathrm{Fe}} = 0.3$, s- and d-wave pair potentials $\Delta_0/\varepsilon_{\mathrm{Fe}} = \Delta_1/\varepsilon_{\mathrm{Fe}} = 0.1$ in Refs. [7,20]. The inset of Fig. 6(a) shows the Fermi surfaces in the $k_y = 0$ plane. We have two Fermi surfaces near the xy plane, and it has a donutlike shape because of the rotational symmetry around the z axis. Figures 6(a)–6(c) show that the dominantly induced components are odd-frequency (spin-triplet and spin-septet) electron/hole pair amplitude (P, $P^{\dagger}$). Namely,

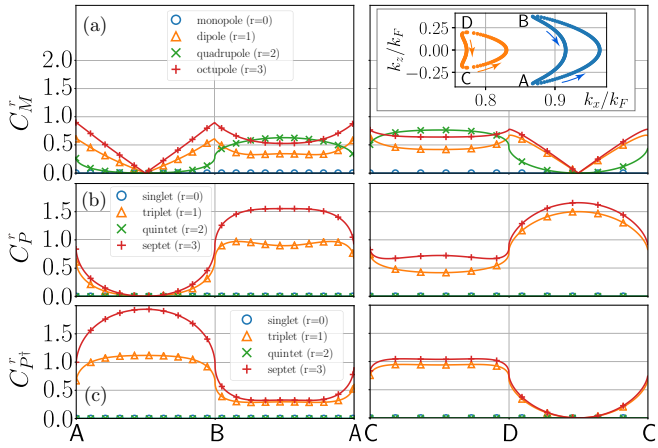

FIG. 6. Wave-vector dependence of (a) $C_M(\boldsymbol{k})$ (multipoles), (b) $C_P(\boldsymbol{k})$, and (c) $C_{P^\dagger}(\boldsymbol{k})$ (multiplet electron and hole pairs) along the Fermi surface in the $j = 3/2$ fermion model. The inset of (a) shows the two Fermi surfaces near the k_x axis located in the $k_y = 0$ plane. The horizontal axis of (a)–(c) is a path shown by arrows in the inset of (a).

the bogolon odd-frequency pair is mainly composed of the electron odd-frequency pair. We note that the diagonal multipole components [M in (a)] also mix with a similar order of magnitudes.

V. SUMMARY

To summarize, we have demonstrated that the nonideal bogolons generate purely odd-frequency pair potential and pair amplitude near the Fermi surface, as different from the usual Fermi liquid of electrons. The odd-frequency pair recovers the original symmetry of the electron system in terms of bogolons, where the broken gauge and time-reversal symmetries are not apparently reflected in the level of the noninteracting Hamiltonian of bogolon. The effect of the odd-frequency pairing is clearly seen in the single-particle spectral functions at low energies where the disorder effect is dominantly present. The system with Bogoliubov Fermi surfaces is a suitable playground for studying the properties of odd-frequency pairing.

Finally, we comment on the remaining issues which are not addressed in this paper. We have discussed the odd-frequency pairing in terms of the symmetry; it is not yet clear how the bogolons' odd-frequency pairing is connected to the topological number defined for the inversion symmetric systems. Furthermore, whereas we deal with the mean-field Hamiltonians which explicitly break the U(1) gauge symmetry, the electron number must be conserved. It is interesting to study the Bogoliubov Fermi surfaces and the odd-frequency pairing in number-conserving framework as in Ref. [72].

ACKNOWLEDGMENTS

This work was supported by JSPS KAKENHI Grants No. JP18K13490, No. JP18H01176, No. JP18H04305, and No. JP19H01842.

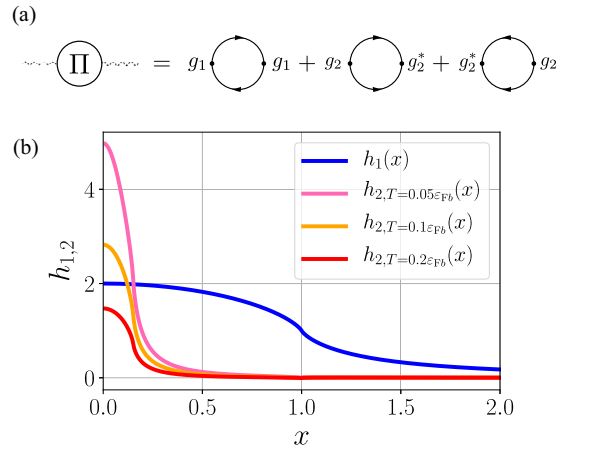

FIG. 7. (a) Self-energy for bosons. (b) Wave-vector dependence of $h_{1,2}$ defined in Eqs. (A9) and (A13) at several temperatures. The cutoff wave vector is chosen as $\omega_C/\varepsilon_{Fb} = 0.3$.

APPENDIX A: INTERACTION WITH BOSONS

The interaction Hamiltonian is defined as Eq. (2) and Eq. (7). With the Hermiticity and inversion symmetry, we obtain the relations similar to Eqs. (4)–(6) for $g_{1,2}(\boldsymbol{k}, \boldsymbol{q})$. The derivation of the self-energies is similar to the standard procedure used in the Fermi liquid theory [64].

1. Boson self-energy

We first derive the boson self-energy. The Green's function of boson is defined by

$$D_{\boldsymbol{q}}(\tau) = -\langle \mathcal{T}\phi_{\boldsymbol{q}}(\tau)\phi_{-\boldsymbol{q}}\rangle, \tag{A1}$$

$$\phi_{\boldsymbol{q}} = \mathrm{i}\sqrt{\frac{\omega_{0,\boldsymbol{q}}}{2}}(b_{\boldsymbol{q}} - b^\dagger_{-\boldsymbol{q}}). \tag{A2}$$

Fourier transformation is given by

$$D_{\boldsymbol{q}}(\mathrm{i}\omega_n) = \int_0^{1/T} d\tau D_{\boldsymbol{q}}(\tau)\mathrm{e}^{\mathrm{i}\omega_n\tau}, \tag{A3}$$

where $\omega_n = 2n\pi T$ is the bosonic Matsubara frequency. The self-energy $\Pi_{\boldsymbol{q}}(\mathrm{i}\omega_n)$ is defined by

$$D_{\boldsymbol{q}}(\mathrm{i}\omega_n)^{-1} = D^0_{\boldsymbol{q}}(\mathrm{i}\omega_n)^{-1} - \Pi_{\boldsymbol{q}}(\mathrm{i}\omega_n), \tag{A4}$$

with the zeroth-order Green's function $D^0_{\boldsymbol{q}}(\mathrm{i}\omega_n) = \omega^2_{0,\boldsymbol{q}}/[(\mathrm{i}\omega_n)^2 - \omega^2_{0,\boldsymbol{q}}]$. The diagrammatic contributions are illustrated in Fig. 7(a) and are then given as follows:

$$\Pi_{\boldsymbol{q}}(\mathrm{i}\omega_n) = \Pi_{1,\boldsymbol{q}}(\mathrm{i}\omega_n) + 2\Pi_{2,\boldsymbol{q}}(\mathrm{i}\omega_n), \tag{A5}$$

$$\Pi_{1,\boldsymbol{q}}(\mathrm{i}\omega_n) = \frac{T}{(2\pi)^3}\sum_m \int d\boldsymbol{k}\, |g_1(\boldsymbol{k}, -\boldsymbol{q})|^2 \times G^0_{\boldsymbol{k}}(\mathrm{i}\varepsilon_m)G^0_{\boldsymbol{k}-\boldsymbol{q}}(\mathrm{i}\varepsilon_m - \mathrm{i}\omega_n), \tag{A6}$$

$$\Pi_{2,\boldsymbol{q}}(\mathrm{i}\omega_n) = -\frac{T}{(2\pi)^3}\sum_m \int d\boldsymbol{k}|g_2(\boldsymbol{k}, -\boldsymbol{q})|^2 G^0_{\boldsymbol{k}}(\mathrm{i}\varepsilon_m) \times \left[G^0_{-\boldsymbol{k}+\boldsymbol{q}}(-\mathrm{i}\varepsilon_m + \mathrm{i}\omega_n) + G^0_{-\boldsymbol{k}+\boldsymbol{q}}(-\mathrm{i}\varepsilon_m - \mathrm{i}\omega_n)\right], \tag{A7}$$

where $G^0_{\boldsymbol{k}}(\mathrm{i}\varepsilon_n)$ is a free particle Green's function of bogolon. First, we find an explicit form of $\Pi_{1,\boldsymbol{q}}(\mathrm{i}\omega_n)$. For the concrete calculation, we introduce the wave-vector-averaged coupling constant $\overline{\Gamma}_{1,\boldsymbol{q}} \equiv \langle|g_1(\boldsymbol{k},-\boldsymbol{q})|^2\rangle_{\boldsymbol{k}}$. Then we obtain the real part of retarded self-energy at low ω as follows:

$$\mathrm{Re}\Pi^{\mathrm{R}}_{1,\boldsymbol{q}}(\omega) = -\frac{\overline{\Gamma}_{1,\boldsymbol{q}} m_b k_{\mathrm{F}b}}{(2\pi)^2} h_1\left(\frac{q}{2k_{\mathrm{F}b}}\right), \tag{A8}$$

where

$$h_1(x) \equiv 1 + \frac{1-x^2}{2x}\ln\left|\frac{1+x}{1-x}\right| \tag{A9}$$

is the Lindhard function shown in Fig. 7(b). We also get the imaginary part as

$$\mathrm{Im}\Pi^{\mathrm{R}}_{1,\boldsymbol{q}}(\omega) = -\frac{\overline{\Gamma}_{1,\boldsymbol{q}} m_b^2}{2\pi q}\omega\theta(2k_{\mathrm{F}b}-q). \tag{A10}$$

These are the same form as those for the usual electrons. On the other hand, in order to calculate $\Pi^{\mathrm{R}}_{2,\boldsymbol{q}}(\omega)$, we introduce the wave-vector-averaged coupling constant $\overline{\Gamma}_{2,\boldsymbol{q}} \equiv \langle|g_2(\boldsymbol{k},-\boldsymbol{q})|^2\rangle_{\boldsymbol{k}}$. The result of the calculation of $\Pi^{\mathrm{R}}_{2,\boldsymbol{q}}(\omega)$ at low ω is as follows:

$$\mathrm{Re}\Pi^{\mathrm{R}}_{2,\boldsymbol{q}}(\omega) = -\frac{\overline{\Gamma}_{2,\boldsymbol{q}} m_b k_{\mathrm{F}b}}{(2\pi)^2} h_{2,T}\left(\frac{q}{2k_{\mathrm{F}b}}\right), \tag{A11}$$

$$\mathrm{Im}\Pi^{\mathrm{R}}_{2,\boldsymbol{q}}(\omega) = -\frac{\overline{\Gamma}_{2,\boldsymbol{q}} m_b^2}{2\pi q}\omega\theta((1+\sqrt{3})k_{\mathrm{F}b}-q), \tag{A12}$$

where

$$h_{2,T}(x) \equiv \int_{\sqrt{1-\omega_{\mathrm{C}}/\varepsilon_{\mathrm{F}b}}}^{\sqrt{1+\omega_{\mathrm{C}}/\varepsilon_{\mathrm{F}b}}} dy \frac{y}{x}\tanh\left(\frac{y^2-1}{2T/\varepsilon_{\mathrm{F}b}}\right) \times \ln\left|\frac{y^2-1+2x^2+2xy}{y^2-1+2x^2-2xy}\right|, \tag{A13}$$

where the energy integration is performed within the cutoff frequency of bosons ω_{C}. We have assumed that the dominant contributions enter at small q. Note that $h_{2,T}(q/2k_{\mathrm{F}b})$ diverges logarithmically in the infrared regime at zero temperature limit. This corresponds to the Cooper instability intrinsic to Fermi surfaces. However, this divergence is suppressed at finite T as shown in Fig. 7(b), in which we are interested.

For later discussion, we derive the explicit form of boson Green's function. The Dyson equation is given as follows:

$$\left[D^{\mathrm{R}}_{\boldsymbol{q}}(\omega)\right]^{-1} = \frac{1}{\omega^2_{0,\boldsymbol{q}}}\left(\omega^2 - \omega^2_{\boldsymbol{q}} - 2\mathrm{i}\omega\gamma_{\boldsymbol{q}}\right), \tag{A14}$$

where

$$\omega_{\boldsymbol{q}} = \omega_{0,\boldsymbol{q}}\sqrt{1-\eta_{\boldsymbol{q}}}, \tag{A15}$$

$$\eta_{\boldsymbol{q}} = \frac{\overline{\Gamma}_{1,\boldsymbol{q}} m_b k_{\mathrm{F}b}}{(2\pi)^2} h_1\left(\frac{q}{2k_{\mathrm{F}b}}\right) + 2\frac{\overline{\Gamma}_{2,\boldsymbol{q}} m_b k_{\mathrm{F}b}}{(2\pi)^2} h_{2,T}\left(\frac{q}{2k_{\mathrm{F}b}}\right), \tag{A16}$$

$$\gamma_{\boldsymbol{q}} = \frac{\overline{\Gamma}_{1,\boldsymbol{q}} m_b^2 \omega^2_{0,\boldsymbol{q}}}{4\pi q}\theta(2k_{\mathrm{F}b}-q) + \frac{\overline{\Gamma}_{2,\boldsymbol{q}} m_b^2 \omega^2_{0,\boldsymbol{q}}}{2\pi q}\theta((1+\sqrt{3})k_{\mathrm{F}b}-q). \tag{A17}$$

Therefore, we get the explicit form of the Green's function as

$$D^{\mathrm{R}}_{\boldsymbol{q}}(\omega) = \frac{\omega^2_{0,\boldsymbol{q}}}{2\omega_{\boldsymbol{q}}}\left(\frac{1}{\omega-\omega_{\boldsymbol{q}}+\mathrm{i}\gamma_{\boldsymbol{q}}} - \frac{1}{\omega+\omega_{\boldsymbol{q}}+\mathrm{i}\gamma_{\boldsymbol{q}}}\right), \tag{A18}$$

which will be used to obtain the bogolon self-energies.

2. Bogolon normal self-energy

Next, we derive the bogolon normal self-energy given in Eq. (10). The diagram of the second-order self-energy is shown in Fig. 2(a). The corresponding self-energy $\Sigma_{\boldsymbol{k}}(\mathrm{i}\varepsilon_n)$ is given as follows:

$$\Sigma_{\boldsymbol{k}}(\mathrm{i}\varepsilon_n) = \Sigma_{1,\boldsymbol{k}}(\mathrm{i}\varepsilon_n) + 2\Sigma_{2,\boldsymbol{k}}(\mathrm{i}\varepsilon_n), \tag{A19}$$

$$\Sigma_{1,\boldsymbol{k}}(\mathrm{i}\varepsilon_n) = -\frac{T}{(2\pi)^3}\sum_m \int d\boldsymbol{k}'\,|g_1(\boldsymbol{k}',\boldsymbol{k}-\boldsymbol{k}')|^2 \times G^0_{\boldsymbol{k}'}(\mathrm{i}\varepsilon_m) D_{\boldsymbol{k}-\boldsymbol{k}'}(\mathrm{i}\varepsilon_n - \mathrm{i}\varepsilon_m), \tag{A20}$$

$$\Sigma_{2,\boldsymbol{k}}(\mathrm{i}\varepsilon_n) = \frac{2T}{(2\pi)^3}\sum_m \int d\boldsymbol{k}'\,|g_2(\boldsymbol{k}',\boldsymbol{k}-\boldsymbol{k}')|^2 \times G^0_{\boldsymbol{k}'}(\mathrm{i}\varepsilon_m) D_{\boldsymbol{k}-\boldsymbol{k}'}(\mathrm{i}\varepsilon_n + \mathrm{i}\varepsilon_m). \tag{A21}$$

We calculate $\Sigma_{1,\boldsymbol{k}}(\mathrm{i}\varepsilon_n)$ at first. For the evaluation of $\Sigma_{\boldsymbol{k}}(\mathrm{i}\varepsilon_n)$, we replace the Matsubara sums by the energy integral. By using the spectral representation for the noninteracting Green's function

$$G^{0,\mathrm{R}}(\boldsymbol{k},\varepsilon) = \int_{-\infty}^{\infty} d\varepsilon' \frac{A^0_{\boldsymbol{k}}(\varepsilon')}{\varepsilon + \mathrm{i}\eta - \varepsilon'}, \tag{A22}$$

the retarded self-energy has the form

$$\Sigma^{\mathrm{R}}_{1,\boldsymbol{k}}(\varepsilon) = \frac{1}{(2\pi)^4}\int d\boldsymbol{k}' \int_{-\infty}^{\infty} d\varepsilon' \int_{-\infty}^{\infty} d\omega \times |g_1(\boldsymbol{k}',\boldsymbol{k}-\boldsymbol{k}')|^2 \frac{A^0_{\boldsymbol{k}'}(\varepsilon')\mathrm{Im}D^{\mathrm{R}}_{\boldsymbol{k}-\boldsymbol{k}'}(\omega)}{\omega+\varepsilon'-\varepsilon-\mathrm{i}\eta} \times \left[\tanh\left(\frac{\varepsilon'}{2T}\right) + \coth\left(\frac{\omega}{2T}\right)\right]. \tag{A23}$$

To evaluate the integral, we again introduce the wave-vector-averaged coupling constant $\overline{\Gamma}_{3,\boldsymbol{k}} \equiv \langle|g_1(\boldsymbol{k}',\boldsymbol{k}-\boldsymbol{k}')|^2\rangle_{\boldsymbol{k}'} \in \mathbb{R}$. Using the variable transformation $\boldsymbol{k}' \to (q, \xi_{\boldsymbol{k}'})$ with $\boldsymbol{q} = \boldsymbol{k} - \boldsymbol{k}'$, we obtain

$$\Sigma^{\mathrm{R}}_{1,\boldsymbol{k}}(\varepsilon) = \frac{\overline{\Gamma}_{3,\boldsymbol{k}} m_b}{(2\pi)^3 k}\int_0^{k_1} dq\, q \int_{-\infty}^{\infty} d\omega \int_{\xi_{|\boldsymbol{k}|-q}}^{\xi_{|\boldsymbol{k}|+q}} d\varepsilon' \times \frac{\mathrm{Im}D^{\mathrm{R}}_{\boldsymbol{q}}(\omega)}{\omega+\varepsilon'-\varepsilon-\mathrm{i}\eta}\left[\tanh\left(\frac{\varepsilon'}{2T}\right) + \coth\left(\frac{\omega}{2T}\right)\right], \tag{A24}$$

where $k_1 = \min\{q_{\mathrm{C}}, 2k_{\mathrm{F}b}\}$, and q_{C} is a wave-vector cutoff of bosons. We can approximate $\xi_{|\boldsymbol{k}|-q}$ and $\xi_{|\boldsymbol{k}|+q}$ by $-\infty$ and $+\infty$, respectively [64]. This procedure is checked for $\varepsilon_{\mathrm{F}b}/\omega_{\mathrm{C}} \gg 1$ by comparing the result with the numerical calculation without using the extrapolation, regardless of the cutoff wave vector k_1. Moreover, we use the relation $\mathrm{Re}D^{\mathrm{R}}_{\boldsymbol{q}}(\omega) = \omega^2_{0,\boldsymbol{q}}/(\omega^2 - \omega^2_{\boldsymbol{q}})$. Then, the real part of $\Sigma^{\mathrm{R}}_{1,\boldsymbol{k}}(\varepsilon)$ is

given as follows:

$$\mathrm{Re}\Sigma^{\mathrm{R}}_{1,\boldsymbol{k}}(\varepsilon) = -\frac{\overline{\Gamma}_{3,\boldsymbol{k}}\zeta}{\omega^*}\varepsilon \tag{A25}$$

for $\varepsilon \ll \omega_{\mathrm{C}}$, where we have introduced the quantities

$$\omega^* = \frac{\displaystyle\int_0^{k_1} dq\, q \frac{\omega^2_{0,\boldsymbol{q}}}{\omega^2_{\boldsymbol{q}}}}{\displaystyle\int_0^{k_1} dq\, q \frac{\omega^2_{0,\boldsymbol{q}}\gamma_{\boldsymbol{q}}}{\omega^4_{\boldsymbol{q}}}}, \tag{A26}$$

$$\frac{\zeta}{\omega^*} = \frac{m_b}{4\pi^2 k_{\mathrm{Fb}}}\int_0^{k_1} dq\, q \frac{\omega^2_{0,\boldsymbol{q}}}{\omega^2_{\boldsymbol{q}}} \tag{A27}$$

to make the notations simple. With $\mathrm{Im}D^{\mathrm{R}}_{\boldsymbol{q}}(\omega) \simeq -2\omega^2_{0,\boldsymbol{q}}\gamma_{\boldsymbol{q}}\omega/\omega^4_{\boldsymbol{q}}$ for $\omega \ll \gamma_{\boldsymbol{q}}$, the imaginary part of $\Sigma^{\mathrm{R}}_{1,\boldsymbol{k}}(\varepsilon)$ is obtained as

$$\mathrm{Im}\Sigma^{\mathrm{R}}_{1,\boldsymbol{k}}(\varepsilon) = -\frac{\overline{\Gamma}_{3,\boldsymbol{k}}\zeta}{\omega^{*2}}(\pi^2T^2 + \varepsilon^2). \tag{A28}$$

The other contribution can also be evaluated with a similar procedure. We list the result below:

$$\Sigma^{\mathrm{R}}_{2,\boldsymbol{k}}(\varepsilon) = -\frac{2\overline{\Gamma}_{4,\boldsymbol{k}}\zeta}{\omega^*}\varepsilon - \mathrm{i}\frac{2\overline{\Gamma}_{4,\boldsymbol{k}}\zeta}{\omega^{*2}}(\pi^2T^2 + \varepsilon^2), \tag{A29}$$

where $\overline{\Gamma}_{4,\boldsymbol{k}} = \langle|g_2(\boldsymbol{k}', \boldsymbol{k}-\boldsymbol{k}')|^2\rangle_{\boldsymbol{k}'} \in \mathbb{R}$.

3. Bogolon anomalous self-energy

In this subsection, we derive the bogolon anomalous self-energy. The diagram of the second-order self-energy is shown in Fig. 2(b). With inversion symmetry, the corresponding self-energy $S^{\dagger}_{\boldsymbol{k}}(\mathrm{i}\varepsilon_n)$ is given as follows:

$$S^{\dagger}_{\boldsymbol{k}}(\mathrm{i}\varepsilon_n) = -\frac{2T}{(2\pi)^3}\sum_m \int d\boldsymbol{k}'\, g^*_1(\boldsymbol{k}', \boldsymbol{k}-\boldsymbol{k}')g^*_2(\boldsymbol{k}', \boldsymbol{k}-\boldsymbol{k}') \times G^0_{\boldsymbol{k}'}(\mathrm{i}\varepsilon_m)[D_{\boldsymbol{k}-\boldsymbol{k}'}(-\mathrm{i}\varepsilon_n + \mathrm{i}\varepsilon_m) - D_{\boldsymbol{k}-\boldsymbol{k}'}(\mathrm{i}\varepsilon_n + \mathrm{i}\varepsilon_m)]. \tag{A30}$$

The explicit form of the retarded self-energy $S^{\dagger\mathrm{R}}_{\boldsymbol{k}}(\varepsilon)$ can be derived by a similar manner to the previous subsection. The result is written as

$$S^{\dagger\mathrm{R}}_{\boldsymbol{k}}(\varepsilon) = -\frac{4\overline{\Gamma}_{5,\boldsymbol{k}}\zeta}{\omega^*}\varepsilon - \mathrm{i}\frac{4\overline{\Gamma}_{5,\boldsymbol{k}}\zeta}{\omega^{*2}}(\pi^2T^2 + \varepsilon^2), \tag{A31}$$

where $\overline{\Gamma}_{5,\boldsymbol{k}} = \langle g^*_1(\boldsymbol{k}', \boldsymbol{k}-\boldsymbol{k}')g^*_2(\boldsymbol{k}', \boldsymbol{k}-\boldsymbol{k}')\rangle_{\boldsymbol{k}'}$.

4. Analytic continuation

For the characterization of the frequency-dependent functional forms, it is suitable to see the physical quantities on the imaginary (or Matsubara) axis. The results on the retarded bogolon self-energies obtained in the previous subsections can be analytically continued to the imaginary axis as

$$\Sigma_{\boldsymbol{k}}(\mathrm{i}\varepsilon_n) = a_{\boldsymbol{k}}\mathrm{i}\varepsilon_n + \mathrm{i}b_{\boldsymbol{k}}[\pi^2T^2 + (\mathrm{i}\varepsilon_n)^2]\mathrm{sgn}\,\varepsilon_n, \tag{A32}$$

$$S^{\dagger}_{\boldsymbol{k}}(\mathrm{i}\varepsilon_n) = c_{\boldsymbol{k}}\mathrm{i}\varepsilon_n + \mathrm{i}d_{\boldsymbol{k}}[\pi^2T^2 + (\mathrm{i}\varepsilon_n)^2]\mathrm{sgn}\,\varepsilon_n, \tag{A33}$$

where

$$a_{\boldsymbol{k}} = -(\overline{\Gamma}_{3,\boldsymbol{k}} + 4\overline{\Gamma}_{4,\boldsymbol{k}})\frac{\zeta}{\omega^*}, \tag{A34}$$

$$b_{\boldsymbol{k}} = \frac{a_{\boldsymbol{k}}}{\omega^*}, \tag{A35}$$

$$c_{\boldsymbol{k}} = -4\overline{\Gamma}_{5,\boldsymbol{k}}\frac{\zeta}{\omega^*}, \tag{A36}$$

$$d_{\boldsymbol{k}} = \frac{c_{\boldsymbol{k}}}{\omega^*}, \tag{A37}$$

from which we can construct both the retarded and advanced Green's functions. The coefficients ω^* and ζ are given in Eqs. (A26) and (A27), and $\overline{\Gamma}_{3,\boldsymbol{k}}$, $\overline{\Gamma}_{4,\boldsymbol{k}}$, $\overline{\Gamma}_{5,\boldsymbol{k}}$ have been defined in the text above. Note that $a_{\boldsymbol{k}}$ and $b_{\boldsymbol{k}}$ are real, while $c_{\boldsymbol{k}}$ and $d_{\boldsymbol{k}}$ are complex.

The electron-electron interaction is also expected to lead to a similar effect discussed above. The imaginary part should be calculated in a manner similar to Ref. [64], and then the real part may be reconstructed through the Kramers-Kronig relation [73,74].

APPENDIX B: CONNECTION TO $j = 3/2$ FERMION MODEL

1. Impurity potential

The impurity scattering term is given in the language of the original electrons by

$$\mathscr{H}_{\mathrm{imp}} = \sum_i \int d\boldsymbol{r} \sum_\eta U_\eta(\boldsymbol{r} - \boldsymbol{R}_i)\vec{c}^{\dagger}(\boldsymbol{r})\hat{O}^\eta\vec{c}(\boldsymbol{r}), \tag{B1}$$

$$\vec{c}(\boldsymbol{r}) = \frac{1}{\sqrt{V}}\sum_{\boldsymbol{k}} \vec{c}_{\boldsymbol{k}}\, \mathrm{e}^{\mathrm{i}\boldsymbol{k}\cdot\boldsymbol{r}}, \tag{B2}$$

where we consider the isotropic ($\eta = 1$) and anisotropic ($\eta = xy, yz, zx, z^2, x^2 - y^2$) scattering centers located at $\boldsymbol{R}_i$, both of which are electric degrees of freedom compatible with nonmagnetic impurities. The full list of 4×4 matrices is defined by using the $\hat{\boldsymbol{J}}$ matrix in Ref. [20]. The impurity position $\boldsymbol{R}_i$ is to be averaged.

The impurity potential can be rewritten in terms of bogolon's operators by using the relation

$$c_{\boldsymbol{k}m} = u^*_{\boldsymbol{k}m}\alpha_{\boldsymbol{k}} + v_{-\boldsymbol{k},m}\alpha^{\dagger}_{-\boldsymbol{k}}, \tag{B3}$$

where only the fermions that have Fermi surfaces are considered in the right-hand side. We then obtain the impurity potential term for bogolons as

$$\mathscr{H}_{\mathrm{imp}} = \frac{1}{V}\sum_{\boldsymbol{k},\boldsymbol{q}} \rho_{\boldsymbol{q}}u_1(\boldsymbol{k}, \boldsymbol{q})\alpha^{\dagger}_{\boldsymbol{k}+\boldsymbol{q}}\alpha_{\boldsymbol{k}} + \frac{1}{V}\sum_{\boldsymbol{k},\boldsymbol{q}} \rho_{\boldsymbol{q}}u_2(\boldsymbol{k}, \boldsymbol{q})\alpha^{\dagger}_{\boldsymbol{k}+\boldsymbol{q}}\alpha^{\dagger}_{-\boldsymbol{k}} + \mathrm{H.c.} + \mathrm{Const.}, \tag{B4}$$

where

$$u_1(\boldsymbol{k}, \boldsymbol{q}) = \sum_\eta \sum_{m,m'} U_\eta(\boldsymbol{q})\left[u_{\boldsymbol{k}+\boldsymbol{q},m}O^\eta_{mm'}u^*_{\boldsymbol{k},m'} - v^*_{\boldsymbol{k},m}O^\eta_{mm'}v_{\boldsymbol{k}+\boldsymbol{q},m'}\right], \tag{B5}$$

$$u_2(\boldsymbol{k}, \boldsymbol{q}) = \sum_\eta \sum_{m,m'} U_\eta(\boldsymbol{q})u_{\boldsymbol{k}+\boldsymbol{q},m}O^\eta_{mm'}v_{-\boldsymbol{k},m'}. \tag{B6}$$

2. Interaction with boson

The interaction term is given in the language of the original electrons by

$$\mathscr{H}_{\rm int} = \frac{\rm i}{\sqrt{V}} \sum_{\eta,\boldsymbol{k},\boldsymbol{q}} g_\eta \sqrt{\frac{\omega^\eta_{0,\boldsymbol{q}}}{2}} (b_{\boldsymbol{q},\eta} - b^\dagger_{-\boldsymbol{q},\eta}) \vec{c}^\dagger_{\boldsymbol{k}+\boldsymbol{q}} \hat{O}^\eta \vec{c}_{\boldsymbol{k}}, \quad \text{(B7)}$$

where the lattice vibration is coupled with the electron charge (isotropic) and orbital moments (anisotropic). Using Eq. (B3), we obtain the interaction term for bogolon as

$$\begin{aligned}\mathscr{H}_{\rm int} = {} & \frac{\rm i}{\sqrt{V}} \sum_{\eta,\boldsymbol{k},\boldsymbol{q}} g_{1,\eta}(\boldsymbol{k},\boldsymbol{q}) \sqrt{\frac{\omega^\eta_{0,\boldsymbol{q}}}{2}} (b_{\boldsymbol{q},\eta} - b^\dagger_{-\boldsymbol{q},\eta}) \alpha^\dagger_{\boldsymbol{k}+\boldsymbol{q}} \alpha_{\boldsymbol{k}} \\ & + \frac{\rm i}{\sqrt{V}} \sum_{\eta,\boldsymbol{k},\boldsymbol{q}} g_{2,\eta}(\boldsymbol{k},\boldsymbol{q}) \sqrt{\frac{\omega^\eta_{0,\boldsymbol{q}}}{2}} (b_{\boldsymbol{q},\eta} - b^\dagger_{-\boldsymbol{q},\eta}) \alpha^\dagger_{\boldsymbol{k}+\boldsymbol{q}} \alpha^\dagger_{-\boldsymbol{k}} \\ & + \text{H.c.}, \end{aligned} \quad \text{(B8)}$$

where

$$g_{1,\eta}(\boldsymbol{k},\boldsymbol{q}) = g_\eta \sum_{m,m'} O^\eta_{mm'} (u_{\boldsymbol{k}+\boldsymbol{q},m} u^*_{\boldsymbol{k},m'} - v^*_{\boldsymbol{k},m} v_{\boldsymbol{k}+\boldsymbol{q},m'}), \quad \text{(B9)}$$

$$g_{2,\eta}(\boldsymbol{k},\boldsymbol{q}) = g_\eta \sum_{m,m'} u_{\boldsymbol{k}+\boldsymbol{q},m} O^\eta_{mm'} v_{-\boldsymbol{k},m'}. \quad \text{(B10)}$$

We have assumed only one of the boson species which gives a dominant contribution at low energies.

3. Interaction among bogolons

Although we focus on the interaction with bosons in this paper, we can also explicitly derive the effective interaction among bogolons. While we expect that the results are similar to the electron-phonon coupling in the weak-coupling approach, as in the Fermi liquid for the usual electrons [64], below we show the explicit form of the interaction among bogolons.

We begin with the contact-type Coulomb interaction among electrons, where the interaction is effectively Yukawa-type due to the Thomas-Fermi screening. The interaction Hamiltonian is written as

$$\mathscr{H}_{\rm C} = \sum_\eta U_\eta \int d\boldsymbol{r} : N^\eta(\boldsymbol{r}) N^\eta(\boldsymbol{r}) :, \quad \text{(B11)}$$

$$N^\eta(\boldsymbol{r}) = \vec{c}^\dagger(\boldsymbol{r}) \hat{O}^\eta \vec{c}(\boldsymbol{r}), \quad \text{(B12)}$$

where $: \cdots :$ is a normal ordering and U_η is a coupling constant. Then we obtain the interaction among bogolons as

$$\begin{aligned}\mathscr{H}_{\rm C} = {} & \sum_{\boldsymbol{k}} U_0(\boldsymbol{k}) \alpha^\dagger_{\boldsymbol{k}} \alpha_{\boldsymbol{k}} + \sum_{\boldsymbol{k}_1,\cdots,\boldsymbol{k}_4} U_1(\boldsymbol{k}_1,\boldsymbol{k}_2,\boldsymbol{k}_3,\boldsymbol{k}_4) \alpha^\dagger_{\boldsymbol{k}_1} \alpha^\dagger_{\boldsymbol{k}_2} \alpha_{\boldsymbol{k}_3} \alpha_{\boldsymbol{k}_4} + \sum_{\boldsymbol{k}_1,\cdots,\boldsymbol{k}_4} U_2(\boldsymbol{k}_1,\boldsymbol{k}_2,\boldsymbol{k}_3,\boldsymbol{k}_4) \alpha^\dagger_{\boldsymbol{k}_1} \alpha^\dagger_{\boldsymbol{k}_2} \alpha^\dagger_{\boldsymbol{k}_3} \alpha_{\boldsymbol{k}_4} + \text{H.c.} \\ & + \sum_{\boldsymbol{k}_1,\cdots,\boldsymbol{k}_4} U_3(\boldsymbol{k}_1,\boldsymbol{k}_2,\boldsymbol{k}_3,\boldsymbol{k}_4) \alpha^\dagger_{\boldsymbol{k}_1} \alpha^\dagger_{\boldsymbol{k}_2} \alpha^\dagger_{\boldsymbol{k}_3} \alpha^\dagger_{\boldsymbol{k}_4} + \text{H.c.}, \end{aligned} \quad \text{(B13)}$$

where

$$\begin{aligned} U_0(\boldsymbol{k}_1) = {} & \frac{1}{V} \sum_{\boldsymbol{k}_2} \sum_{\eta,m_1,\cdots,m_4} U_\eta O^\eta_{m_1m_4} O^\eta_{m_2m_3} (u_{\boldsymbol{k}_1,m_1} v^*_{\boldsymbol{k}_1,m_2} u^*_{\boldsymbol{k}_2,m_3} v_{\boldsymbol{k}_2,m_4} - u_{\boldsymbol{k}_1,m_1} v^*_{-\boldsymbol{k}_2,m_2} u^*_{\boldsymbol{k}_1,m_3} v_{-\boldsymbol{k}_2,m_4} \\ & + u_{\boldsymbol{k}_1,m_1} v^*_{-\boldsymbol{k}_2,m_2} v_{-\boldsymbol{k}_2,m_3} u^*_{\boldsymbol{k}_1,m_4} - v^*_{-\boldsymbol{k}_2,m_1} u_{-\boldsymbol{k}_2,m_2} u^*_{\boldsymbol{k}_1,m_3} v_{\boldsymbol{k}_1,m_4} - v^*_{\boldsymbol{k}_1,m_1} u_{\boldsymbol{k}_1,m_2} u^*_{\boldsymbol{k}_2,m_3} v_{\boldsymbol{k}_2,m_4} + v^*_{-\boldsymbol{k}_2,m_1} u_{\boldsymbol{k}_1,m_2} u^*_{\boldsymbol{k}_1,m_3} v_{-\boldsymbol{k}_2,m_4} \\ & + v^*_{\boldsymbol{k}_2,m_1} u_{\boldsymbol{k}_2,m_2} v_{\boldsymbol{k}_1,m_3} u^*_{\boldsymbol{k}_1,m_4} - v^*_{-\boldsymbol{k}_2,m_1} u_{\boldsymbol{k}_1,m_2} v_{-\boldsymbol{k}_2,m_3} u^*_{\boldsymbol{k}_1,m_4} - v^*_{-\boldsymbol{k}_2,m_1} v^*_{\boldsymbol{k}_1,m_2} v_{\boldsymbol{k}_1,m_3} v_{-\boldsymbol{k}_2,m_4} + v^*_{-\boldsymbol{k}_2,m_1} v^*_{\boldsymbol{k}_1,m_2} v_{-\boldsymbol{k}_2,m_3} v_{\boldsymbol{k}_1,m_4} \\ & + v^*_{\boldsymbol{k}_1,m_1} v^*_{-\boldsymbol{k}_2,m_2} v_{\boldsymbol{k}_1,m_3} v_{-\boldsymbol{k}_2,m_4} - v^*_{\boldsymbol{k}_1,m_1} v^*_{-\boldsymbol{k}_2,m_2} v_{-\boldsymbol{k}_2,m_3} v_{\boldsymbol{k}_1,m_4}), \end{aligned} \quad \text{(B14)}$$

$$\begin{aligned} U_1(\boldsymbol{k}_1,\boldsymbol{k}_2,\boldsymbol{k}_3,\boldsymbol{k}_4) = {} & \frac{1}{V} \sum_{\eta,m_1,\cdots,m_4} U_\eta O^\eta_{m_1m_4} O^\eta_{m_2m_3} (u_{\boldsymbol{k}_1,m_1} u_{\boldsymbol{k}_2,m_2} u^*_{\boldsymbol{k}_3,m_3} u^*_{\boldsymbol{k}_4,m_4} + u_{\boldsymbol{k}_1,m_1} v^*_{\boldsymbol{k}_3,m_2} u^*_{\boldsymbol{k}_4,m_3} v_{\boldsymbol{k}_2,m_4} - u_{\boldsymbol{k}_1,m_1} v^*_{\boldsymbol{k}_3,m_2} v_{\boldsymbol{k}_2,m_3} u^*_{\boldsymbol{k}_4,m_4} \\ & - v^*_{\boldsymbol{k}_3,m_1} u_{\boldsymbol{k}_1,m_2} u^*_{\boldsymbol{k}_4,m_3} v_{\boldsymbol{k}_2,m_4} + v^*_{\boldsymbol{k}_3,m_1} u_{\boldsymbol{k}_1,m_2} v_{\boldsymbol{k}_2,m_3} u^*_{\boldsymbol{k}_4,m_4} + v^*_{\boldsymbol{k}_3,m_1} v^*_{\boldsymbol{k}_4,m_2} v_{\boldsymbol{k}_1,m_3} v_{\boldsymbol{k}_2,m_4}) \delta_{\boldsymbol{k}_1+\boldsymbol{k}_2,\boldsymbol{k}_3+\boldsymbol{k}_4}, \end{aligned} \quad \text{(B15)}$$

$$\begin{aligned} U_2(\boldsymbol{k}_1,\boldsymbol{k}_2,\boldsymbol{k}_3,\boldsymbol{k}_4) = {} & \frac{1}{V} \sum_{\eta,m_1,\cdots,m_4} U_\eta O^\eta_{m_1m_4} O^\eta_{m_2m_3} (u_{\boldsymbol{k}_1,m_1} u_{\boldsymbol{k}_2,m_2} v_{\boldsymbol{k}_3,m_3} u^*_{\boldsymbol{k}_4,m_4} - u_{\boldsymbol{k}_1,m_1} u_{\boldsymbol{k}_2,m_2} u^*_{\boldsymbol{k}_4,m_3} v_{\boldsymbol{k}_3,m_4} \\ & + u_{\boldsymbol{k}_1,m_1} v^*_{\boldsymbol{k}_4,m_2} v_{\boldsymbol{k}_2,m_3} v_{\boldsymbol{k}_3,m_4} - v^*_{\boldsymbol{k}_4,m_1} u_{\boldsymbol{k}_1,m_2} v_{\boldsymbol{k}_2,m_3} v_{\boldsymbol{k}_3,m_4}) \delta_{\boldsymbol{k}_1+\boldsymbol{k}_2+\boldsymbol{k}_3,\boldsymbol{k}_4}, \end{aligned} \quad \text{(B16)}$$

and

$$U_3(\boldsymbol{k}_1,\boldsymbol{k}_2,\boldsymbol{k}_3,\boldsymbol{k}_4) = \frac{1}{V} \sum_{\eta,m_1,\cdots,m_4} U_\eta O^\eta_{m_1m_4} O^\eta_{m_2m_3} u_{\boldsymbol{k}_1,m_1} u_{\boldsymbol{k}_2,m_2} v_{\boldsymbol{k}_3,m_3} v_{\boldsymbol{k}_4,m_4} \delta_{\boldsymbol{k}_1+\boldsymbol{k}_2+\boldsymbol{k}_3+\boldsymbol{k}_4,0}. \quad \text{(B17)}$$

The one-body part can be included in the kinetic energy $\xi_{\boldsymbol{k}}$ in Eq. (1). Here $\alpha^{\dagger}_{\boldsymbol{k}}\alpha^{\dagger}_{-\boldsymbol{k}}$ like terms become zero by inversion symmetry. The presence of U_2 and U_3 is characteristic and generic for the effective interaction among bogolons.

Note that, for a quantitative discussion, we need to consider the fact that interaction parameters are renormalized for effective low-energy model. This procedure can be performed by a manner similar to the constrained random phase approximation (cRPA) technique [75] as done in the study of the low-energy effective model in correlated electron systems from first-principles calculation. It would be an interesting future problem to derive these interactions among bogolons by starting from a microscopic Hamiltonian of the original electrons.

4. Single-particle spectral function

We connect the single particle spectrum of the electrons to that of the bogolons. We define the single-particle spectrum for $j = 3/2$ electrons by

$$A^{\rm elec}_{\boldsymbol{k}}(\varepsilon) = \frac{1}{2\pi f(\varepsilon)} \int_{-\infty}^{\infty} dt \langle \vec{\psi}^{\dagger}_{\boldsymbol{k}} \vec{\psi}_{\boldsymbol{k}}(t)\rangle e^{i\varepsilon t}, \tag{B18}$$

where we have introduced the Nambu spinor $\vec{\psi}_{\boldsymbol{k}} = (\vec{c}^{\rm T}_{\boldsymbol{k}}, \vec{c}^{\dagger}_{-\boldsymbol{k}})^{\rm T}$. This is written in terms of bogolons, and near the Fermi level it has the form

$$\begin{aligned} A^{\rm elec}_{\boldsymbol{k}}(\varepsilon) &= \frac{1}{2\pi f(\varepsilon)} \int_{-\infty}^{\infty} dt [\langle \alpha^{\dagger}_{\boldsymbol{k}}\alpha_{\boldsymbol{k}}(t)\rangle + \langle \alpha_{-\boldsymbol{k}}\alpha^{\dagger}_{-\boldsymbol{k}}(t)\rangle] e^{i\varepsilon t} \\ &= -\frac{1}{\pi} {\rm Im\,Tr}\, \hat{G}^{\rm R}_{\boldsymbol{k}}(\varepsilon), \end{aligned} \tag{B19}$$

where the 2×2 matrix $\hat{G}^{\rm R}_{\boldsymbol{k}}(\varepsilon)$ is the retarded version of the Green's function written in Eq. (10).

[1] N. N. Bogoliubov, Sov. Phys. JETP **34**, 41 (1958).
[2] G. E. Volovik, Phys. Lett. A **142**, 282 (1989).
[3] G. E. Volovik, JETP Lett. **58**, 469 (1993).
[4] W. V. Liu and F. Wilczek, Phys. Rev. Lett. **90**, 047002 (2003).
[5] E. Gubankova, E. G. Mishchenko, and F. Wilczek, Phys. Rev. Lett. **94**, 110402 (2005); Phys. Rev. B **74**, 184516 (2006).
[6] S. Autti, J. T. Mäkinen, J. Rysti, G. E. Volovik, V. V. Zavjalov, and V. B. Eltsov, Phys. Rev. Research **2**, 033013 (2020).
[7] D. F. Agterberg, P. M. R. Brydon, and C. Timm, Phys. Rev. Lett. **118**, 127001 (2017).
[8] P. M. R. Brydon, D. F. Agterberg, H. Menke, and C. Timm, Phys. Rev. B **98**, 224509 (2018).
[9] N. F. Q. Yuan and L. Fu, Phys. Rev. B **97**, 115139 (2018).
[10] S. Sumita, T. Nomoto, K. Shiozaki, and Y. Yanase, Phys. Rev. B **99**, 134513 (2019).
[11] H. Menke, C. Timm, and P. M. R. Brydon, Phys. Rev. B **100**, 224505 (2019).
[12] J. M. Link, I. Boettcher, and I. F. Herbut, Phys. Rev. B **101**, 184503 (2020).
[13] J. M. Link and I. F. Herbut, Phys. Rev. Lett. **125**, 237004 (2020).
[14] C. J. Lapp, G. Börner, and C. Timm, Phys. Rev. B **101**, 024505 (2020).
[15] C. Setty, Y. Cao, A. Kreisel, S. Bhattacharyya, and P. J. Hirschfeld, Phys. Rev. B **102**, 064504 (2020).
[16] Y. Sato, S. Kasahara, T. Taniguchi, X. Xing, Y. Kasahara, Y. Tokiwa, Y. Yamakawa, H. Kontani, T. Shibauchi, and Y. Matsuda, Proc. Nat. Acad. Sci. USA **115**, 1227 (2018).
[17] C. Setty, S. Bhattacharyya, Y. Cao, A. Kreisel, and P. J. Hirschfeld, Nat. Commun. **11**, 523 (2020).
[18] For a review, see T. Shibauchi, T. Hanaguri, and Y. Matsuda, J. Phys. Soc. Jpn. **89**, 102002 (2020).
[19] H. Oh and E.-G. Moon, Phys. Rev. B **102**, 020501(R) (2020).
[20] S.-T. Tamura, S. Iimura, and S. Hoshino, Phys. Rev. B **102**, 024505 (2020).
[21] C. Timm, P. M. R. Brydon, and D. F. Agterberg, Phys. Rev. B **103**, 024521 (2021).
[22] I. F. Herbut and J. M. Link, Phys. Rev. B **103**, 144517 (2021).
[23] V. L. Berezinskii, JETP Lett. **20**, 287 (1974).
[24] T. R. Kirkpatrick and D. Belitz, Phys. Rev. Lett. **66**, 1533 (1991).
[25] D. Belitz and T. R. Kirkpatrick, Phys. Rev. B **46**, 8393 (1992).
[26] A. Balatsky and E. Abrahams, Phys. Rev. B **45**, 13125 (1992).
[27] V. J. Emery and S. Kivelson, Phys. Rev. B **46**, 10812 (1992).
[28] J. R. Schrieffer, A. V. Balatsky, E. Abrahams, and D. J. Scalapino, J. Supercond. **7**, 501 (1994).
[29] F. S. Bergeret, A. F. Volkov, and K. B. Efetov, Rev. Mod. Phys. **77**, 1321 (2005).
[30] Y. Tanaka, M. Sato, and N. Nagaosa, J. Phys. Soc. Jpn. **81**, 011013 (2012).
[31] J. Linder and A. V. Balatsky, Rev. Mod. Phys. **91**, 045005 (2019).
[32] For a review, J. Cayaoa, C. Triola, and A. M. Black-Schaffer, Eur. Phys. J.: Spec. Top. **229**, 545 (2020).
[33] A. V. Balatsky and J. Bonča, Phys. Rev. B **48**, 7445 (1993).
[34] Y. Fuseya, H. Kohno, and K. Miyake, J. Phys. Soc. Jpn. **72**, 2914 (2003).
[35] T. Hotta, J. Phys. Soc. Jpn. **78**, 123710 (2009).
[36] K. Shigeta, S. Onari, K. Yada, and Y. Tanaka, Phys. Rev. B **79**, 174507 (2009).
[37] K. Shigeta, Y. Tanaka, K. Kuroki, S. Onari, and H. Aizawa, Phys. Rev. B **83**, 140509 (2011).
[38] M. Vojta and E. Dagotto, Phys. Rev. B **59**, R713(R) (1999).
[39] K. Yada, S. Onari, Y. Tanaka, and K. Miyake, arXiv:0806.4241.
[40] Y. Yanagi, Y. Yamashita, and K. Ueda, J. Phys. Soc. Jpn. **81**, 123701 (2012).
[41] H. Kusunose, Y. Fuseya, and K. Miyake, J. Phys. Soc. Jpn. **80**, 044711 (2011).
[42] P. Coleman, E. Miranda, and A. Tsvelik, Phys. Rev. Lett. **70**, 2960 (1993).
[43] P. Coleman, E. Miranda, and A. Tsvelik, Phys. Rev. B **49**, 8955 (1994).
[44] O. Zachar, S. A. Kivelson, and V. J. Emery, Phys. Rev. Lett. **77**, 1342 (1996).
[45] J. Otsuki, Phys. Rev. Lett. **115**, 036404 (2015).

[46] A. M. Tsvelik, Proc. Natl. Acad. Sci. USA **116**, 12729 (2019).
[47] V. J. Emery and S. A. Kivelson, Phys. Rev. Lett. **71**, 3701 (1993).
[48] M. Jarrell, H. Pang, and D. L. Cox, Phys. Rev. Lett. **78**, 1996 (1997).
[49] S. Hoshino and Y. Kuramoto, Phys. Rev. Lett. **112**, 167204 (2014).
[50] S. Hoshino, Phys. Rev. B **90**, 115154 (2014).
[51] H. Kusunose, J. Phys. Soc. Jpn. **85**, 113701 (2016).
[52] F. B. Anders, Phys. Rev. B **66**, 020504(R) (2002).
[53] F. B. Anders, Eur. Phys. J. B **28**, 9 (2002).
[54] R. Heid, Z. Phys. B **99**, 15 (1995).
[55] D. Belitz and T. R. Kirkpatrick, Phys. Rev. B **60**, 3485 (1999).
[56] D. Solenov, I. Martin, and D. Mozyrsky, Phys. Rev. B **79**, 132502 (2009).
[57] H. Kusunose, Y. Fuseya, and K. Miyake, J. Phys. Soc. Jpn. **80**, 054702 (2011).
[58] Ya. V. Fominov, Y. Tanaka, Y. Asano, and M. Eschrig, Phys. Rev. B **91**, 144514 (2015).
[59] F. S. Bergeret, A. F. Volkov, and K. B. Efetov, Phys. Rev. Lett. **86**, 4096 (2001).
[60] M. Eschrig, J. Kopu, J. C. Cuevas, and G. Schön, Phys. Rev. Lett. **90**, 137003 (2003).
[61] Y. Tanaka and A. A. Golubov, Phys. Rev. Lett. **98**, 037003 (2007).
[62] Y. Tanaka, Y. Tanuma, and A. A. Golubov, Phys. Rev. B **76**, 054522 (2007).
[63] Z. Faraei and S. A. Jafari, Phys. Rev. B **100**, 035447 (2019).
[64] A. A. Abrikosov, L. P. Gorkov, and I. E. Dzyaloshinski, *Methods of Quantum Field Theory in Statistical Physics* (Dover, New York, 1975).
[65] L. F. Feiner, J. H. Jefferson, and R. Raimondi, Phys. Rev. B **53**, 8751 (1996).
[66] F. Yang and M. W. Wu, Phys. Rev. B **102**, 014511 (2020).
[67] P. Coleman, A. M. Tsvelik, N. Andrei, and H. Y. Kee, Phys. Rev. B **60**, 3608 (1999).
[68] R. Flint, M. Dzero, and P. Coleman, Nat. Phys. **4**, 643 (2008).
[69] S. Iimura, M. Hirayama, and S. Hoshino, Phys. Rev. B **100**, 094532 (2019).
[70] A. J. Leggett, *Quantum Liquids: Bose Condensation and Cooper Pairing in Condensed-Matter Systems* (Oxford University Press, Oxford, 2006).
[71] A. I. Coldea, S. F. Blake, S. Kasahara, A. A. Haghighirad, M. D. Watson, W. Knafo, E. S. Choi, A. McCollam, P. Reiss, T. Yamashita, M. Bruma, S. C. Speller, Y. Matsuda, T. Wolf, T. Shibauchi, and A. J. Schofield, npj Quant. Mater. **4**, 2 (2019).
[72] Y. Lin and A. J. Leggett, arXiv:1803.08003.
[73] K. Miyake, T. Matsuura, and C. M. Varma, Solid State Commun. **71**, 1149 (1989).
[74] A. C. Jacko, J. O. Fjærestad, and B. J. Powell, Nat. Phys. **5**, 422 (2009).
[75] F. Aryasetiawan, M. Imada, A. Georges, G. Kotliar, S. Biermann, and A. I. Lichtenstein, Phys. Rev. B **70**, 195104 (2004).